Structure and morphology of the MATLAS dwarf galaxies and their central nuclei

Mélina Poulain, Francine Marleau, Rebecca Habas, Pierre-Alain Duc, Rubén Sánchez-Janssen, Patrick Durrell, Sanjaya Paudel, Syeda Lammim Ahad, Abhishek Chougule, Oliver Müller, et al.

Monthly Notices of the ROYAL ASTRONOMICAL SOCIETY

MNRAS **506,** 5494–5511 (2021) https://doi.org/10.1093/mnras/stab2092
Advance Access publication 2021 July 22

Structure and morphology of the MATLAS dwarf galaxies and their central nuclei

Mélina Poulain,[1★] Francine R. Marleau,[1] Rebecca Habas,[2] Pierre-Alain Duc,[2] Rubén Sánchez-Janssen,[3] Patrick R. Durrell,[4] Sanjaya Paudel,[5] Syeda Lammim Ahad,[6] Abhishek Chougule,[7,8] Oliver Müller,[2] Sungsoon Lim,[9] Michal Bílek[10] and Jérémy Fensch[11]

[1]*Institute für Astro- und Teilchenphysik, Universität Innsbruck, Technikerstraße 25/8, A-6020 Innsbruck, Austria*
[2]*CNRS, Observatoire Astronomique, Université de Strasbourg, 11, rue de l'Université. F-67000 Strasbourg, France*
[3]*UK Astronomy Technology Centre, Royal Observatory Edinburgh, Blackford Hill, Edinburgh EH9 3HJ, UK*
[4]*Department of Physics, Astronomy, Geology, and Environmental Sciences, Youngstown State University, Youngstown, OH 44555 USA*
[5]*Department of Astronomy and Center for Galaxy Evolution Research, Yonsei University, Seoul 03722, Republic of Korea*
[6]*Leiden Observatory, Leiden University, PO Box 9513, NL-2300 RA Leiden, the Netherlands*
[7]*Instituto de Astrofísica e Ciências do Espaço, CAUP, Universidade do Porto, Rua das Estrelas, P-4150-762 Porto, Portugal*
[8]*Departamento de Física e Astronomia, Faculdade de Ciências, Universidade do Porto, Rua do Campo Alegre 687, P-4169-007 Porto, Portugal*
[9]*Department of Astronomy, Yonsei University, 50 Yonsei-ro Seodaemun-gu, Seoul 03722, Republic of Korea*
[10]*Nicolaus Copernicus Astronomical Center, Polish Academy of Sciences, Bartycka 18, PL-00-716 Warsaw, Poland*
[11]*CNRS, Centre de Recherche Astrophysique de Lyon, UMR5574, ENS de Lyon, Univ. Lyon, Univ. Lyon 1, F-69007 Lyon, France*

Accepted 2021 July 16. Received 2021 July 16; in original form 2021 January 28

ABSTRACT

We present a photometric study of the dwarf galaxy population in the low to moderate density environments of the MATLAS (Mass Assembly of early-Type gaLAxies with their fine Structures) deep imaging survey. The sample consists of 2210 dwarfs, including 508 nucleated. We define a nucleus as a compact source that is close to the galaxy photocentre (within 0.5 R_e) which is also the brightest such source within the galaxy's effective radius. The morphological analysis is performed using a 2D surface brightness profile modelling on the *g*-band images of both the galaxies and nuclei. Our study reveals that, for similar luminosities, the MATLAS dwarfs show ranges in the distribution of structural properties comparable to cluster (Virgo and Fornax) dwarfs and a range of sizes comparable to the Local Group and Local Volume dwarfs. Colour measurements using the *r*- and *i*-band images indicate that the dwarfs in low and moderate density environments are as red as cluster dwarfs on average. The observed similarities between dwarf ellipticals in vastly different environments imply that dEs are not uniquely the product of morphological transformation due to ram-pressure stripping and galaxy harassment in high density environments. We measure that the dwarf nuclei are located predominantly in massive, bright and round dwarfs and observe fewer nuclei in dwarfs with a faint centre and a small size. The colour of the galaxy nucleus shows no clear relation to the colour of the dwarf, in agreement with the migration and wet migration nucleus formation scenarios. The catalogues of the MATLAS dwarfs photometric and structural properties are provided.

Key words: galaxies: dwarf – galaxies: nuclei – galaxies: photometry – galaxies: structure.

1 INTRODUCTION

Galaxy structure and morphology is one of the most fundamental ways used to characterize galaxies and infer their formation scenario. These structural properties are found to be correlated with the physical properties of the galaxy, such as their star formation rate, merging history, and overall scale. When observed over a range of cosmic time, they can also be used as a tool for measuring galaxy evolution. Although the morphological nomenclature across galaxies of all luminosity (or mass) have similarities, there is a clear distinction between the so-called 'massive' and 'dwarf' galaxies. While the morphology and structure of massive galaxies have been studied in equal measure over a wide range of environments, this is not the case for dwarf galaxies. Indeed, the characterization of their structure and morphology have relied until very recently almost entirely, due to their low surface brightness, on those found in the Local Group (LG; McConnachie 2012) and nearby clusters (Virgo: Ferrarese et al. 2012; Fornax: Eigenthaler et al. 2018; Venhola et al. 2019).

The morphological types of dwarf galaxies have been found to belong to two main groups: elliptical/spheroidal (dE/dSph), the most commonly observed type (Ferguson & Binggeli 1994), and irregular (dI; van den Bergh 1960). The dIs, typically located in the outskirts of groups and clusters, are gas-rich galaxies with ongoing star formation. They are physically similar to irregular galaxies and thus can be defined as their low-mass end (Grebel 2004). The dEs/dSphs are gas-poor galaxies and, until recently, generally observed in dense environment like groups and clusters (Ferguson & Sandage 1991). The dSphs are usually defined as the low-luminosity end of the elliptical dwarfs and have so far mostly been observed in the LG (Grebel 2001).

★ E-mail: melina.poulain@student.uibk.ac.at, melina.poulain45@gmail.com

In the last decades, many discussions concerning the formation scenarios of dEs have been carried out, with an emphasis on two distinct processes. The first process involves environmental effects like the harassment/ram-pressure stripping of late-type galaxies, either bright spiral galaxies or dIs. Some studies have shown the tendency of bright spiral galaxies to change morphologically and become more compact when going through harassment inside clusters (Moore et al. 1996; Mastropietro et al. 2005; Aguerri & González-García 2009). Other models describe the evolution of dIs through external processes such as ram-pressure stripping (Boselli et al. 2008) or tidal interactions (Mayer et al. 2001; Pasetto, Chiosi & Carraro 2003). The second scenario suggests a formation caused by internal processes (Dekel & Silk 1986). It is supported by the results from simulations of isolated dwarf galaxies (Valcke et al. 2008; Sawala et al. 2010) as well as the relations observed between dEs and bright ellipticals structural properties in clusters and the LG (Adami et al. 2006; Misgeld, Mieske & Hilker 2008).

A significant fraction of the dwarfs, called nucleated dwarfs, contains a central compact nucleus. The origin of these nuclei is still unclear. Possible formation scenario suggests that the nuclear star cluster (NSC) forms from accreted gas at the centre of the galaxy (*in situ* scenario; Loose, Kruegel & Tutukov 1982). Another proposes that an NSC is formed by globular clusters (GCs) that migrate towards the centre and merge due to dynamical frictions (migration scenario; Tremaine, Ostriker & Spitzer 1975). Simulations combined to observations show that a combination of both processes is necessary to reconstruct the observed NSCs in dwarfs and more massive galaxies (Bekki 2007; Antonini et al. 2012; Ordenes-Briceño et al. 2018; Sills et al. 2019). However, the level of contribution from each process seems to vary with the mass of the host galaxy, with the infalling GCs scenario dominating in galaxies with a stellar mass below 10^9 $M_\odot$ due to the shorter dynamical friction time-scales (Turner et al. 2012; Sánchez-Janssen et al. 2019; Fahrion et al. 2020; Neumayer, Seth & Boeker 2020). A third formation model of the nucleus has been proposed by Guillard, Emsellem & Renaud (2016) for dwarfs galaxies. Called the wet migration scenario, it combines the *in situ* and migration scenarios by considering an off-centred formation and growth of a massive cluster which then migrates to the centre while retaining part of its gas. This migration can then be followed by a merger with another cluster. Dwarf galaxies are also known to host active galactic nuclei (AGNs; e.g, Marleau, Clancy & Bianconi 2013; Marleau et al. 2017; Kaviraj, Martin & Silk 2019; Mezcua & Domínguez Sánchez 2020; Molina et al. 2021) or both NSC and AGNs (Côté et al. 2006; den Brok et al. 2015).

Due to their shallow gravitational potential wells, dwarf galaxies are expected to be more affected by the environment than more massive galaxies. The possible effects of the environment on the structural properties as well as on the formation scenarios have been studied during the last decades. Comparison of the scaling relations for dwarfs in clusters and in the LG support a picture where the dwarfs are shaped more by internal than external processes (Weisz et al. 2011; Young et al. 2014; Dunn 2015). Some formation scenarios, such as the transformation of late-type galaxies to dEs via harassment, have been put forward to explain the morphology–density relation of dwarf galaxies (Ferguson & Sandage 1991). However, these works mainly focused on the dwarf galaxies in clusters and in the LG. Some studies have looked for dwarf galaxies in the field and nearby groups environments in the Local Volume (LV; Sharina et al. 2008; Müller, Jerjen & Binggeli 2017, 2018; Carlsten et al. 2020). But without a large sample of dwarfs in low-density environments, the role of the environment cannot be properly estimated.

The study by Habas et al. (2020) of 2210 dwarf galaxies, beyond the LV, in the low to medium-density environments of the MATLAS (Mass Assembly of early-Type gaLAxies with their fine Structures) survey (Duc et al. 2014) started to address this problem. In this paper, we present the results of a detailed structural and morphological analysis of this large sample of field dwarf galaxies. The paper is organized as follows. In Section 2, we present the MATLAS survey and the dwarfs sample. In Section 3, we detail the galaxy modelling method. The structural and photometric properties of the MATLAS dwarfs are presented in Section 4. In Section 5, we describe and show the results of the study of the central compact nuclei. In Section 6, we discuss the results, and conclude in Section 7.

2 THE MATLAS DWARF GALAXY SAMPLE

The MATLAS survey is associated to the ATLAS^{3D} project (Cappellari et al. 2011). This project aims to study the kinematic and structural properties of a complete sample of 260 nearby early-type galaxies (ETGs). The galaxies were selected so they have an absolute magnitude $M_K < -21.5$ and are situated at $D \lesssim 45$ Mpc, $|\delta - 29°| < 35°$, and $|b| > 15°$ where D is the distance, δ is the declination, and b the Galactic latitude. The ATLAS ^{3D} observations have been performed in radio with the Westerbork Radio Synthesis Telescope (WRST), in millimetre with the IRAM 30-m telescope and the Combined Array for Research in Millimeter-wave Astronomy (CARMA), and in optical with the Canada–France–Hawaii telescope (CFHT). They are combined to spectroscopic observations from the Spectroscopic Areal Unit for Research on Optical Nebulae (SAURON) integral-field unit of the William Herschel Telescope (WHT), numerical simulations, and semi-analytical models of galaxy formation.

The MATLAS survey, coupled to the Next Generation Virgo Cluster Survey (NGVS; Ferrarese et al. 2012), focused on the deep optical observations from the CFHT. The NGVS ETGs, situated in the Virgo cluster, were observed from 2009 to 2013 over an area of 104 deg^2. The dwarfs detected in the NGVS are being studied in a series of independent papers (e.g. Sánchez-Janssen et al. 2016, 2019; Ferrarese et al. 2020). The ETGs outside the Virgo cluster, located in low to moderate density environments, were observed for the MATLAS survey from 2012 to 2015.

The MATLAS survey aims to study the low surface brightness structures of the 202 ETGs situated outside the Virgo cluster. Rejecting the galaxies close to bright stars, the observations were carried out over 150 fields containing 180 ETGs and 55 late-type galaxies (LTGs) using the MegaCam camera. The data are composed of $1° \times 1°$ images for 150, 148, and 78 fields in the g, r, and i bands, respectively, as well as additional u-band observations for the 12 closest targets ($D < 20$ Mpc). The images have a resolution of 0.19 arcsec/pixel and, in the g band, a seeing between 0.5 and 1.61 arcsec and a depth in surface brightness of 28.5–29 mag arcsec^{-2} (Duc et al. 2014). As it has the largest number of fields observed, the g-band observations have been primarily used for our analysis. The complete list of observed bands for each MATLAS target is available in Habas et al. (2020).

As the MATLAS survey allows us to study low surface brightness structures thanks to its deep imaging, it has provided a unique data set to search and identify a statistically significant number of dwarf galaxies in low-density environments. Two methods were used to identify the dwarf candidates: a visual inspection coupled to a semi-automated catalogue of candidates. The visual inspection was performed over the 150 fields available in the g band. Each field was studied by at least one of the team members and galaxies with extended central light concentration or spiral structures was

Table 1. Structural and photometric properties of the MATLAS dwarfs.

ID	Host ETG		Distance (Mpc)		RA (deg)	Dec. (deg)	m_g	$(g-i)_0$	$(g-r)_0$	n	R_e (arcsec)	b/a	PA	$\mu_{0,g}$ (mag/arcsec^2)	$\langle\mu_{e,g}\rangle$ (mag/arcsec^2)	Morph
(1)	(2)	(3)	(4)	(5)	(6)	(7)	(8)	(9)	(10)	(11)	(12)	(13)	(14)	(15)	(16)	(17)
MATLAS-1	NGC 0448	29.5	1	–	18.2998	−2.0792	–	–	–	–	–	–	–	–	–	dI
MATLAS-2	NGC 0448	29.5	1	–	18.3236	−1.1708	19.90	0.71	–	1.21	3.81	0.45	1.35	23.26	24.05	dE
MATLAS-3	NGC 0448	29.5	1	–	18.3396	−1.8231	20.44	–	–	0.61**	4.54	0.52	85.42	24.18	24.96	dI
MATLAS-4	NGC 0448	29.5	1	–	18.4198	−1.9169	–	–	–	–	–	–	–	–	–	dI
MATLAS-5	NGC 0448	29.5	1	–	18.6778	−1.0972	20.55	0.72	0.50	1.33	3.52	0.75	38.52	23.74	24.52	dE
MATLAS-6	NGC 0448	29.5	1	–	18.6875	−1.2415	19.95	0.58	–	0.69	3.88	0.75	46.88	23.35	24.14	dE
MATLAS-7	NGC 0448	29.5	1	28.96[a]	18.7193	−1.0953	–	–	–	–	–	–	–	–	–	dE
MATLAS-8	NGC 0448	29.5	1	–	18.7567	−1.4806	19.63	1.26	0.75	0.57	8.75	0.78	48.37	24.79	25.58	dEN
MATLAS-9	NGC 0448	29.5	1	–	18.7782	−1.2741	–	–	–	–	–	–	–	–	–	dIN
MATLAS-10	NGC 0448	29.5	1	–	18.7949	−1.4718	17.27	–	–	1.09	4.45	0.82	31.35	20.98	21.76	dEN
...	...	...	...	...	...	...	...	...	...	...	...	...	...	...	...	...

Notes. The full table is available as supplementary material as well as at CDS. Columns meanings: (1) Dwarf ID; (2) Assumed host ETG; (3) Distance; (4) Distance flag: 1 = one single massive Atlas^{3D} galaxy in the field with distance; 2 = several massive Atlas3D galaxies in the field all located at roughly the same distance; 3 = several massive Atlas^{3D} galaxies in the field with a majority at roughly the same distance, but some discrepant one(s); 4 = several massive Atlas3D galaxies in the field with a range of distances; (5) Distance measurement from [(a)] SDSS DR13 database, [(b)] Poulain et al., in preparation, [(c)] Ann, Seo & Ha (2015), [(d)] Karachentsev, Makarov & Kaisina (2013), [(e)] Müller et al. (2021); (6) and (7) Right ascension and declination of the dwarf; (8) Apparent magnitude in the g band; (9) $g-i$ colour corrected for Galactic extinction; (10) $g-r$ colour corrected for Galactic extinction; (11) Sérsic index (12) Effective radius; (13) Axis-ratio; (14) Position angle; (15) Central surface brightness in the g-band; (16) Average surface brightness within R_e in the g-band; (17) Dwarf morphology.
dE$*$ corresponds to the dwarf whose nucleus matches with a star in the *Gaia* DR2 catalogue.
dE$**$ corresponds to the dwarf for which one of the central bright GCs is possibly an NSC (Forbes et al. 2019).
** Corresponds to a Sérsic index derived on a binned image.

rejected to avoid contamination by background lenticulars or spirals. A catalogue of 1349 candidates was obtained after this first step. To create the semi-automated catalogue, the software SOURCE EXTRACTOR (Bertin & Arnouts 1996) was run on the *g*-band images as well as on RMEDIAN filtered images (Secker 1995) which emphasize the extended low surface brightness objects and removes small bright objects. Only sources detected in both images were selected. A cut in average surface brightness, apparent magnitude, and size was then applied. The photometric selection criteria for the automated selection algorithm were defined based on the visual catalogue, while the size was set such that dwarf candidates were reliably differentiated from background galaxies. The initial visual catalogue was cross-matched against the semi-automated catalogue, and any candidates not detected by SOURCE EXTRACTOR were appended to the semi-automated catalogue, generating a sample of 25 522 galaxies. The final list of dwarf candidates was created after two visual inspections of the data; in the first, potential dwarf galaxies were identified by a minimum of three team members, which were then inspected a second time by five team members to produce a final clean sample. All the details on the selection method can be found in Habas et al. (2020).

This produced a final catalogue of 2210 dwarf galaxies with 73.4 per cent of ellipticals (dEs) and 26.6 per cent of irregulars (dIs). In the entire catalogue, 23.2 per cent of the dwarfs are nucleated. We will now refer to this sample as the MATLAS dwarfs. We note that the dI sample is likely not complete due to the possible confusion between dwarf irregular galaxies and a background galaxies. As explained in Habas et al. (2020), a small number of galaxies with hints of spiral structure were rejected from the dwarf sample as likely background galaxies, but were later found to have absolute magnitudes M_g indicating they are dwarf galaxies, based on pre-existing distance estimates. These galaxies were not added back into the sample.

An important parameter, not obtainable from the CFHT images, is the distance to the dwarfs. It allows us, for example, to confirm the dwarf nature of our galaxies and to compute physical sizes and luminosities. Using spectroscopic redshifts and H I measurements, distances were measured for 13.5 per cent of the catalog (the H I properties of the dwarf galaxies will be discussed in an upcoming paper, Poulain et al. in preparation). Considering a cut in M_g of -18, the dwarf nature of the candidates was confirmed for 99 per cent of the dwarfs for which a distance could be computed. Distances from available surveys allowed to measure relative velocities suggesting that ∼90 per cent of the 13.5 per cent form as satellite population around the nearest massive galaxies. For this subsample of dwarfs with distances, it was also shown that assuming the dwarfs are satellites of the targeted massive ETG located near the centre of each field is nearly as accurate (∼80 per cent) as matching them with the nearest massive galaxy in 3D space; thus, for the full sample, we have assumed that the MATLAS dwarfs are satellites located at the same distance as the targeted massive ETG. And therefore, unless a distance measurement is available, we will use that distance for each dwarf. However, some fields contain several ETGs with different distances, causing uncertainties on the host of the dwarf and its distance. The dwarfs for which there is an ambiguity in the distance have been flagged in Table 1.

3 GALAXY MODELLING

The galaxy modelling was performed on the *g*-band images using the software GALFIT (Peng et al. 2010). We applied a 2D Sérsic model (Sérsic 1963) to estimate the surface brightness profiles of the dwarfs. For each dwarf, we have produced a cutout image using as a side length, a multiple of the effective radius (R_e) of the galaxy as estimated by SOURCE EXTRACTOR. We looked for a size of the cutout that would provide the best sky background estimate, i.e. that would allow us to keep sufficient background without including many surrounding bright sources. A sample of 16 dwarf galaxies belonging to the MegaCam field was used for this analysis. For each dwarf, we produced several cutouts with sizes ranging from 5 to 15R_e and estimated the sky background value for each of them. We found that these values converged at 9 times the effective radius and therefore postage stamps were cut at 9R_e. On average, this corresponds to an image of approximately 1 arcmin on each side. We then extracted the PSF image of each field using PSFEx (Bertin 2011) and performed a first Sérsic fit of our candidates with SOURCE EXTRACTOR in order to get a first estimate of the structural parameters. These were then used as input parameters in a Sérsic fit with GALFIT.

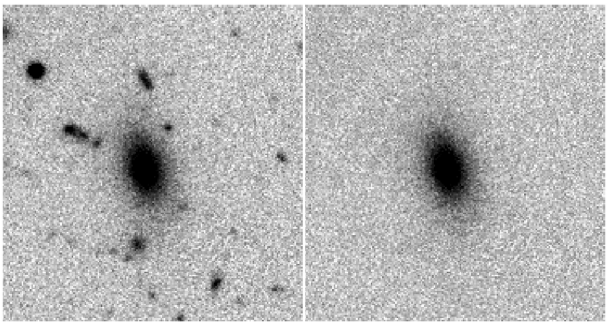

Figure 1. Example of the cleaning of foreground stars and background galaxies for a dE. The cutouts are 37 arcsec × 37 arcsec with North up and East left.

3.1 Image cleaning

GALFIT is not designed to separate individual sources, and therefore light from nearby sources (either point-like or extended) can impact the quality of the modelling. This is especially problematic for the faint dwarfs in our sample. To prevent such contamination, we applied patches to remove sources from the cutouts used for the GALFIT modelling. To do this, we created a noise-model image, which is our base for the patching, as we will use part of it to mask the undesired sources. This image is composed of the addition of the first Sérsic model from GALFIT to a grid of background noise estimated from the cutout.

Our cleaning consists of replacing the bright sources by the corresponding area of pixels from the noise-model image. To detect the bright sources that fall either on top of the galaxy or close to it and may therefore affect the fit, we first ran the DAOPHOT algorithm (Stetson 1987) above one effective radius of the dwarf. We applied a first cleaning using circular regions of radius 1 arcsec as patches. Then, we ran SOURCE EXTRACTOR to detect all remaining bright sources on the cut-out image and patched the extended sources, essentially composed of stars with haloes and background galaxies, more distant than 2R_e using the SOURCE EXTRACTOR segmentation image.

We obtained a good result for about two thirds of the galaxies, of which an example can be seen in Fig. 1. For the remaining dwarfs, the cleaning was not sufficient due to a bad first estimate of the model by GALFIT or a poor estimate of the size of the detected sources by SOURCE EXTRACTOR. To fix this problem, we had to proceed with a manual cleaning using the image patching tool of

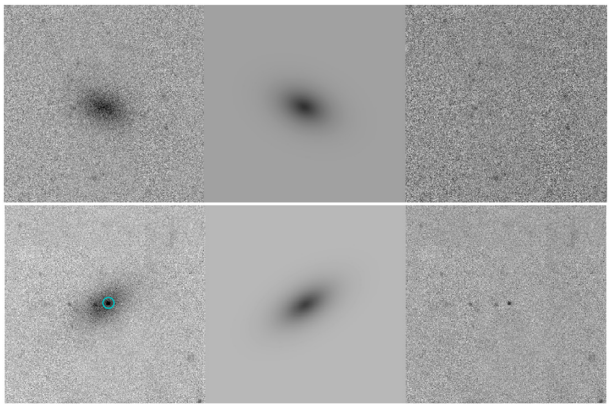

Figure 2. Top: Sérsic modelling of a dE. Bottom: Masked Sérsic modelling of a dE,N. The mask (cyan) is visible on the cutout (left) image. Left: Cleaned cutout. Middle: Model. Right: Residual image. The cutouts are 48 arcsec × 48 arcsec with North up and East left.

the software GAIA (GRAPHICAL ASTRONOMY AND IMAGE ANALYSIS TOOL; Draper et al. 2014).

After this cleaning, we performed a second Sérsic fit, of which an example is visible in Fig. 2. For our sample of nucleated dwarfs, to obtain the properties of the diffuse part of the galaxy, we executed a masked Sérsic fit as well as a double profile (a Sérsic coupled with a PSF or King profile) fit. For the masked Sérsic fit, we created a pixel mask at the centre of the galaxies with a circle of area 50 pixels^2, which corresponds to a radius ∼1.3 arcsec. This size was a good compromise to mask the nucleus without masking a too large part of the dwarf. We gave this mask as input to GALFIT to perform the Sérsic model. The double profile fit will be discussed later is Section 5. Combining the results from both types of fit, we obtained a GALFIT model of the diffuse part for 84 per cent of our nucleated sample. For most of the nucleated dwarfs without a GALFIT model, the bad fits are caused by similar features as the non-nucleated dwarfs (see Section 3.2).

3.2 Image resolution

Spatially binning the images can enhance the visibility of the dwarfs. For this reason, 3 × 3 binned images (0.56 arcsec pixel^{-1}) were used for the dwarf selection process (Section 2). For the sample of nucleated dwarfs, as we wanted the best resolution for the nuclei, we have used the unbinned images (0.19 arcsec pixel^{-1}). To determine which image resolution is the best to produce a good Sérsic model of the non-nucleated dwarfs, we have run GALFIT on both resolution images. We could obtain a model for 1164 and 1005 galaxies using the binned and unbinned images, respectively. Models could only be obtained in both images for 978 dwarfs.

We have compared the structural parameters (Sérsic index, apparent magnitude, effective radius, and axial ratio) of the dwarfs having a model from both image resolution (see Fig. 3). All parameters but one are independent of the resolution of the modelled image. The Sérsic index has a strong dependence to the type of image, as the strength of the effect of binning seems to increase with the Sérsic index value. This is likely due to the fact that the resulting smoothing enhances the central surface brightness of the dwarfs with a bright centre. This effect explains in part why we could obtain some models using binned images only, as on the unbinned image the galaxy would appear too faint to be correctly fitted by GALFIT.

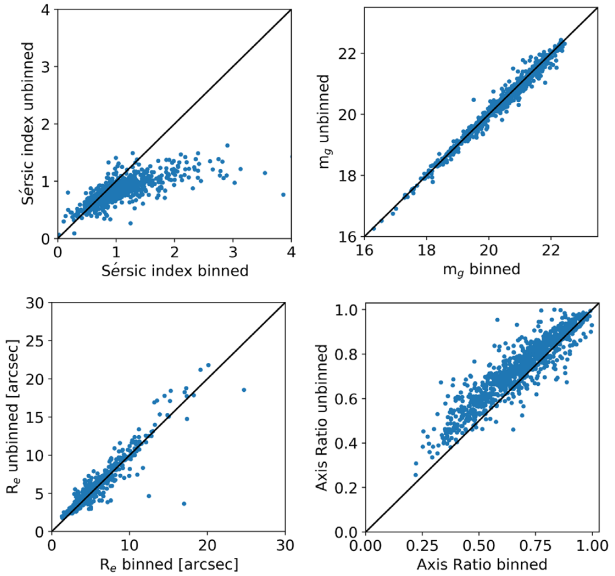

Figure 3. Comparison of the obtained Sérsic index, m_g, R_e, and axial ratio with image resolution used for the model fit. Black line: both axis are equal. The Sérsic index shows a strong dependence on the resolution of the image.

Table 2. Results of the modelling of the MATLAS dwarfs for each morphology and according to the resolution of the images used.

Morphology	Number of dwarfs	Dwarfs with model	Unbinned model	Binned model
dE	1181	1022	892	130
dI	522	142	116	26
dE,N	453	415	415	–
dI,N	54	10	10	–

Due to a better modelling of the inner regions, our final sample of dwarf GALFIT properties is based on the unbinned images, unless the fits failed in which case we used the successful GALFIT results from the binned images (156 galaxies). As the Sérsic indices were not accurately recovered for the binned images, we excluded them from future analysis. In total, for the non-nucleated dwarf galaxies, we could model 1164 (68 per cent) objects in the sample. The bad modelling is mainly caused by the presence of structures like star-forming regions, especially inside the irregular galaxies which, coupled with the irregular shape, result in only 27 per cent of the dIs having a GALFIT model. Other reasons, pertaining mainly to the dwarf ellipticals, are the presence of a bright centre or the too faint luminosity of the galaxy. As a consequence, 87 per cent of the dEs were modeled. A summary of the results of the modelling for each morphology and according to the resolution of the images used is available in Table 2.

4 THE STRUCTURAL AND PHOTOMETRIC PROPERTIES OF THE MATLAS DWARFS

We present here the structural properties of 1022 dEs, 142 dIs, 415 dE,N, and 10 dI,N through scaling relations and parameter distributions. The distributions of absolute and apparent magnitude of the modelled MATLAS dwarfs are presented in Fig. 4. The structural and photometric properties of the dwarfs can be found in Table 1. We compare them to the LG, LV, and cluster dwarf galaxies.

4.1 Catalogues of dwarfs

We obtained catalogues of dwarfs from the LG, the LV, and select clusters from the literature to use as comparison samples. For the LG, we used the catalogue from McConnachie (2012) which summarizes the properties of the LG dwarfs. For the LV, we obtained the catalogue from Carlsten et al. (2020), a study of the properties of 155 dwarfs located around 10 LV hosts based on data from the CFHT. To represent the cluster environment, we utilized dwarfs samples from the two nearby Virgo and Fornax clusters. The Virgo cluster dwarfs catalogue comes from the NGVS, introduced in Section 2, and focuses on the core (inner one virial radius, R_{vir}) of the cluster. We chose two surveys to characterize the Fornax cluster dwarf population: the Next Generation Fornax survey (NGFS; Eigenthaler et al. 2018) and the Fornax Deep survey (FDS; Venhola et al. 2018). The first makes use of observations from the Dark Energy Camera of the 4-meter Blanco telescope in the *u*, *g*, *i* bands and the second is based on data from the VLT Survey telescope (VST) in the *u*, *g*, *r*, *i* bands. Both telescopes show similar seeing to the CFHT. These surveys are complementary, as the NGFS focuses on the inner part of the Fornax cluster (within ∼0.25 R_{vir}) while the FDS studies the entire cluster, with galaxies located within and beyond the cluster virial radius. As a consequence, the first includes only dEs, while the second is composed of both dEs and dIs.

4.2 Comparison with dwarf galaxies from different environments

Three scaling relations were presented in Habas et al. (2020) (fig. 11) for a sample of 1470 MATLAS dwarfs.[1] These plots show that the MATLAS dwarfs are similar to dwarf galaxies in clusters and the LG in term of size (effective radius), luminosity (absolute magnitude), and surface brightness. We derived the *g*-band surface brightnesses (central $\mu_{0,g}$; at R_e $\mu_{e,g}$; and within R_e $\langle\mu_{e,g}\rangle$) of the modelled dwarfs based on the equations from Graham & Driver (2005), based on the total magnitude and effective radius returned by GALFIT. We show in Fig. 5 the relation between M_g and R_e for a sightly larger sample, including parameters of 119 additional galaxies (mainly dE,N) that we compare with an additional sample of dwarfs from the LV (Carlsten et al. 2020). As in Habas et al. (2020), the region defined by the MATLAS dwarfs is precisely overlapping the clusters and LG. Moreover, it also overlaps the LV dwarfs. This result means that the environment does not dramatically alter the scaling relations, at least in a statistical sense. Focusing on the morphologies of the MATLAS dwarfs, we can see that both dEs and dIs have the same range of luminosities and sizes. However, as is visible in Fig. 4, only faint dIs have been successfully modelled, and thus may introduce a bias regarding the results.

To investigate the similarities of the structural properties of dwarf populations located in low to high density environments, we focus our study on the distribution of each individual structural property. We use the results of the modelling of the 1589 MATLAS dwarfs and compare the Sérsic index, effective radius, and axial ratio to the ones measured for the Virgo (NGVS; Ferrarese et al. 2020) and Fornax (NGFS: Eigenthaler et al. 2018; FDS: Venhola et al. 2018) dwarfs with the same absolute magnitude. We divide the MATLAS sample in two absolute magnitude bins, from −17 to −12 and from −12 to −8, where −17 is the brightest common absolute magnitude bin between the samples and −12 is the median M_g of the MATLAS

[1]With the use of unbinned and binned images for the modelling of the nucleated and non-nucleated population, respectively.

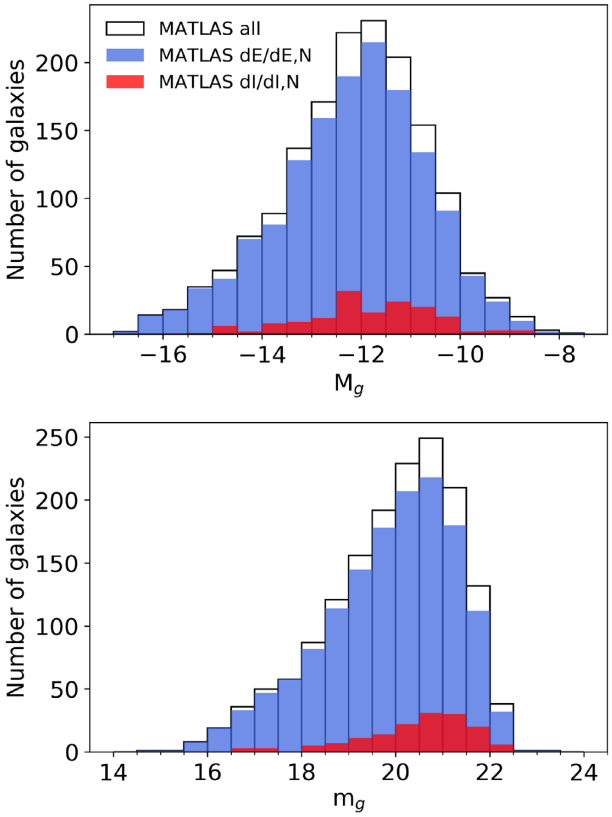

Figure 4. Distribution of M_g and m_g of the modelled MATLAS dwarfs for the full sample (empty bars), the dEs (blue) and the dIs (red).

sample (see Fig. 6). One can see that the MATLAS and cluster dwarfs show similar structural properties, with the bright dwarfs showing a broader range of Sérsic index and effective radius than the faint ones.

To test if the distributions of each property of the MATLAS and cluster dwarfs are drawn from a common distribution, we have performed two-sample Kolmogorov−Smirnov (KS) tests on the two absolute magnitude bins of bright ($M_g = -17$ to -12) and faint ($M_g = -12$ to -8) dwarfs. The null hypothesis is that the two samples come from the same distribution, and we set a significance level of $\alpha = 0.05$. We report the obtained *p*-values in Table 3. We split our analysis considering on one side the dwarfs located in the core of clusters (the NGFS and NGVS samples) and on the other side dwarfs in the whole cluster (the FDS sample). In the cluster core, based on the *p*-values, we cannot reject the hypothesis that the properties are drawn from the same population as the ones of the MATLAS dwarfs when considering: (1) the Sérsic index of all NGFS dwarfs, NGVS faint dwarfs, (2) the axial ratio of all dwarfs, and (3) the effective radius of NGFS faint dwarfs and NGVS bright dwarfs. But, we reject the null hypothesis for: (1) the Sérsic index of NGVS bright dwarfs, and (2) the effective radius of NGFS bright dwarfs, NGVS faint dwarfs. Thus, in the core of clusters, the *p*-values of most of the properties of the bright and faint dwarfs suggest that these galaxies are likely drawn from the same population as the MATLAS dwarfs, implying the possibility of a similar formation scenario for these galaxies. However, we find a different result when looking at the whole Fornax cluster dwarf population, as we reject the null hypothesis for all the properties but the Sérsic index of the faint dwarfs. This suggests that even though the dwarfs in the core of clusters possibly share the same formation background as the

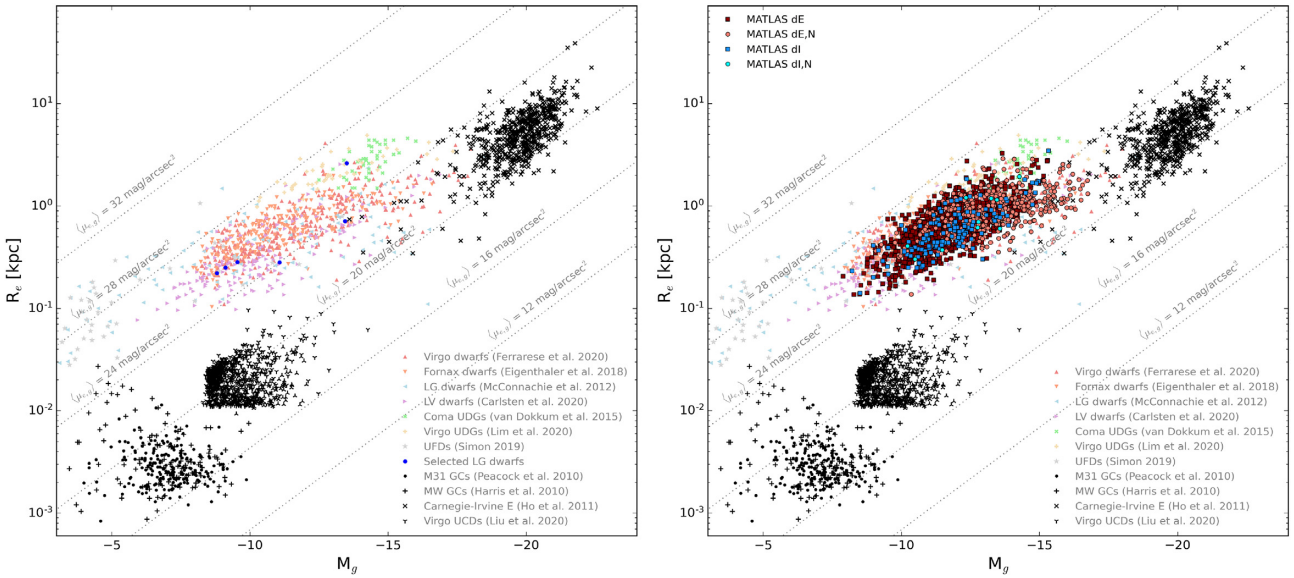

Figure 5. Scaling relation comparing the MATLAS dwarfs with the ones from clusters (NGVS, NGFS), the LG and the LV. We show the dwarfs together with ultradiffuse galaxies (van Dokkum et al. 2015; Lim et al. 2020), ultra-faint dwarfs (Simon 2019), globular clusters (Harris 2010; Peacock et al. 2010), massive elliptical galaxies (Ho et al. 2011) and ultracompact dwarfs (Liu et al. 2020) for comparison. Left: scaling relation without the MATLAS dwarfs. Some well-known dwarfs from the LG are highlighted with blue dots. Right: Scaling relation with the MATLAS dwarfs. The region defined by the MATLAS dwarfs is precisely overlapping the clusters, LG and LV dwarfs.

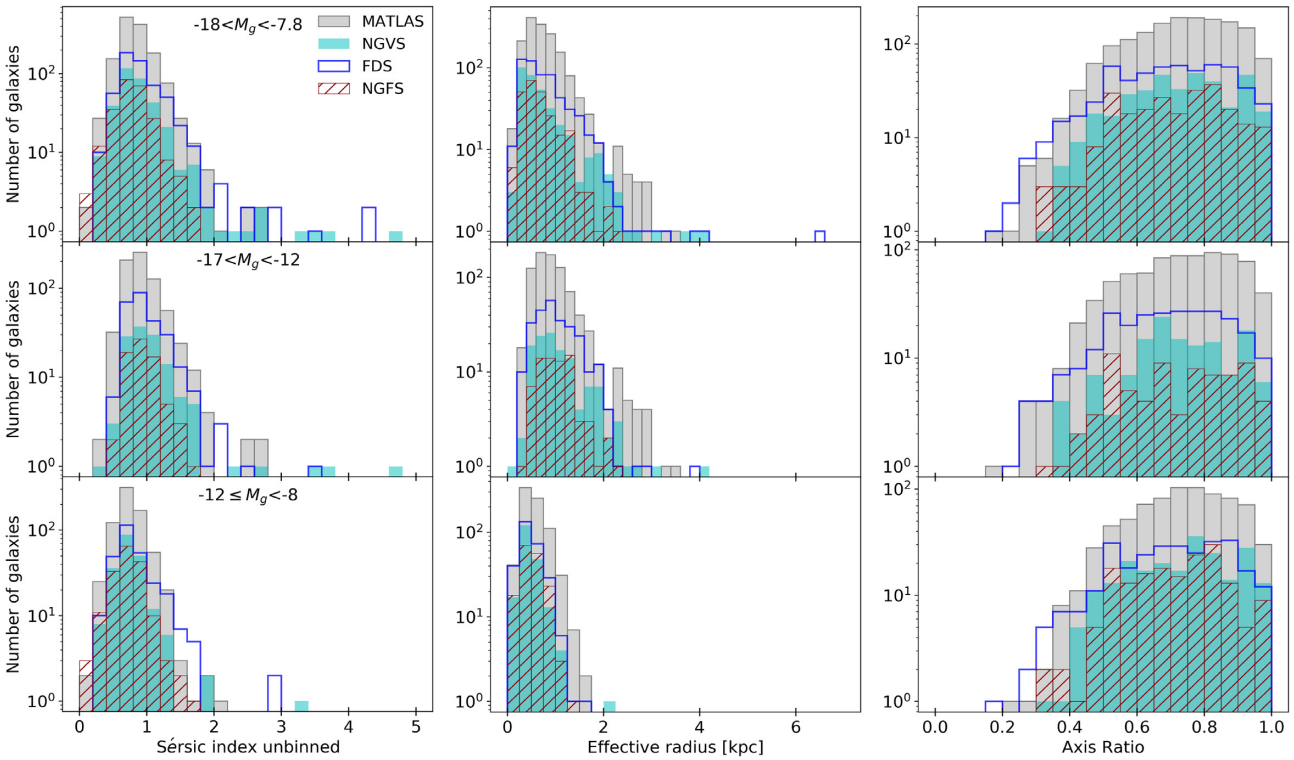

Figure 6. Comparison of distribution of the structural properties of the modelled MATLAS dwarfs with the ones from NGVS, NGFS, and FDS per absolute magnitude range. Top: complete samples. Middle: bright dwarfs with $-17 < M_g < -12$. Bottom: faint dwarfs with $-12 \leq M_g < -8$. Due to the large difference of statistics between the MATLAS distributions and the others, we display the counts in log scale to ensure a better visibility. The MATLAS and cluster dwarfs show similar ranges of structural properties.

MATLAS dwarfs, it may not be the case for all the dwarfs in the cluster environment.

4.3 Colours of the MATLAS dwarfs

To obtain the colours of the galaxies successfully modelled in the *g* band, we ran the exact same model on the *i*- and *r*-band images, leaving only the magnitude and sky values free to change in the input parameters of GALFIT. Fewer fields have available observations in the *i* and *r* bands than in the *g* band, thus we obtained a GALFIT model for 782 and 1307 dwarfs in the *i* and *r* band, respectively.

To look for the influence of the environment on the dwarfs colours and compare the stellar population according to their morphology of the MATLAS dwarfs, we compare our samples with dwarfs located in high and medium to low density environments. To perform a more robust comparison, we limit the selected samples to the ones observed with the filters of MegaCam on the CFHT. Therefore, we are comparing the MATLAS dwarfs to those from the NGVS (Sánchez-Janssen et al. 2019) and to dwarfs in the LV situated around isolated galaxies or in groups (Carlsten et al. 2020). We present colour–magnitude relations (CMRs; Bell et al. 2004) for the Galactic extinction corrected[2] $(g-r)_0$ and $(g-i)_0$ colours in Fig. 7. To be consistent in our comparison, all the magnitudes are issued from single Sérsic modelling (i.e. for the nucleated dwarfs, the nuclei were masked or modelled by a PSF or King profile). The CMRs are divided according to morphological type with the dEs at the top, the dE,N in the middle, and the dIs, dI,N at the bottom. To ensure a better visibility of the dE populations' colours of MATLAS and NGVS, we computed the running average of the colours, represented by dashed lines. We note that, in contrary to the nuclei (see Section 5.3), we do not indicate the GALFIT statistical error on the colour of the dwarfs, as the error bars would appear smaller than the size of the marker. Focusing on the $(g-i)_0$ colour, the MATLAS dEs, dE,N, and dIs have a median colour of 0.70 ± 0.20, 0.82 ± 0.22, and 0.55 ± 0.23, respectively. While the MATLAS dEs, dE,N, and dIs have a median $(g-r)_0$ colour of 0.46 ± 0.16, 0.54 ± 0.13, and 0.36 ± 0.18, respectively. Looking at the different morphologies, we note that dE,N show redder colours than dEs and that dIs appear to be bluer than dEs. Comparing the MATLAS dwarfs to the ones from the Virgo cluster and the LV, one can see that for all morphological types, the dwarfs are showing similar colours, independently of their local environment, meaning that the MATLAS dEs are, on average, as red as clusters dwarfs. This result contradicts the findings of simulations (Mistani et al. 2016) and observations (Haines, Gargiulo & Merluzzi 2008; Geha et al. 2012) that star-forming, blue, dwarf galaxies are found in majority in low-density environments. We also note that the obtained colours are consistent with measurements from different instruments in groups (Müller et al. 2017, 2018) and in the Fornax cluster (Venhola et al. 2019).

4.4 The structural properties of the MATLAS nucleated dwarfs

In the high density environment of the Virgo and Fornax clusters' core, populated by dEs, about 30 per cent of the dwarf galaxies show a central nucleus (Ordenes-Briceño et al. 2018; Sánchez-Janssen et al. 2019). However, only 3 dwarf galaxies of the LG show a central nuclei: the M31 satellites NGC 205 and M32 (Kent 1987; Lauer et al. 1998; Mateo 1998; Butler & Martínez-Delgado 2005; De Rijcke et al. 2006) and the MW satellite Sagittarius dSph (Mateo 1998; Monaco et al. 2005; Bellazzini et al. 2008). In the MATLAS sample, about 23 per cent of the dwarfs are nucleated (Section 2) with ∼10 per cent of the irregulars and ∼39 per cent of the ellipticals. The MATLAS dE sample shows a slightly larger fraction of nucleated than in Virgo and Fornax clusters, which is consistent given the less restrictive offset criteria chosen for the nucleus definition (see Section 5). A first study of the nucleated sample, looking at the fraction of nucleated of the MATLAS dwarfs as a function of M_g, has been done in Habas et al. (2020). The results are in agreement with the findings in the Virgo and Fornax clusters, i.e. that the brighter dwarf galaxies tend to be more nucleated. In this section, we focus on four parameters of the nucleated dwarf population (absolute magnitude, Sérsic index, effective radius, and axial ratio) that we compare to the non-nucleated population.

In the scaling relation of Fig. 5, the nucleated population of the MATLAS sample is represented in blue while the non-nucleated one is in red. We see a trend of the nucleated dwarfs to be larger and brighter than the non-nucleated ones. To look more in detail at this trend, we compare the distributions of structural parameters of these two dwarf populations. To avoid any possible biases from the dI population, we consider here only the dEs. In Fig. 8 are represented the distributions of the absolute magnitude, Sérsic index, effective radius, and axial ratio. As seen in the top left panel, the non-nucleated, and nucleated population have different ranges of M_g, with the nucleated dwarfs being brighter. The structural properties of the nucleated dwarfs are compared to those of the non-nucleated dwarfs within the same absolute magnitude range, i.e. $-15.5 \leq M_g < -9$. We observe in all cases a shift of the distributions peaks between the nucleated (in cyan) and non-nucleated (in blue) dwarfs. These differences mean that nucleated are rounder than non-nucleated dwarfs and that we observe less nuclei in dwarfs with a faint center (i.e. a Sérsic index < 1) and a small size (i.e. a $R_e < 1$ kpc). A similar trend has also been noted for Fornax and Virgo dwarfs (Sánchez-Janssen et al. 2016; Eigenthaler et al. 2018).

5 THE PROPERTIES OF THE COMPACT CENTRAL NUCLEI

The nucleated dwarf galaxies and their nuclei have mainly been studied in the environment of clusters (Coma, Virgo and Fornax, den Brok et al. 2014; Ordenes-Briceño et al. 2018; Sánchez-Janssen et al. 2019) and nearby groups (Georgiev et al. 2009; Fahrion et al. 2020). In this section, we investigate the properties of the nuclei of the MATLAS dwarfs, located in low-to-moderate density environments, as compared to clusters dwarf nuclei. We define a nucleus as a compact source near the dwarf photocentre (within $\sim 0.5 R_e$, Section 5.3) that appears to be the brightest compact source within the galaxy's effective radius. When two to three-point sources of similar magnitude were located close to the galaxy photocentre and appeared brighter than the surrounding point sources, we defined them as multiple nuclei (see Section 5.5). This selection gave us a sample of 508 nucleated dwarf candidates. As NSCs in dwarfs can have a similar magnitude to the brightest globular clusters, we have estimated the probability of a nuclei to actually be confused with a globular cluster projected near the centre of the dwarf. The Monte Carlo simulation used for this purpose is described in Appendix A1. The probability that a bright GC is found near the centre of the dwarf depends on the distance of the dwarf which determines how many GCs will be above the detection limit. When the nucleated dwarfs are located at distances $\leq$20 Mpc [$>$20 Mpc], we compute a probability of contamination $\lesssim$10 per cent for galaxy photocentre separations below 0.5 arcsec [below 1.5 arcsec]. A contamination of our sample

[2]The extinction corrections are from Schlafly & Finkbeiner (2011).

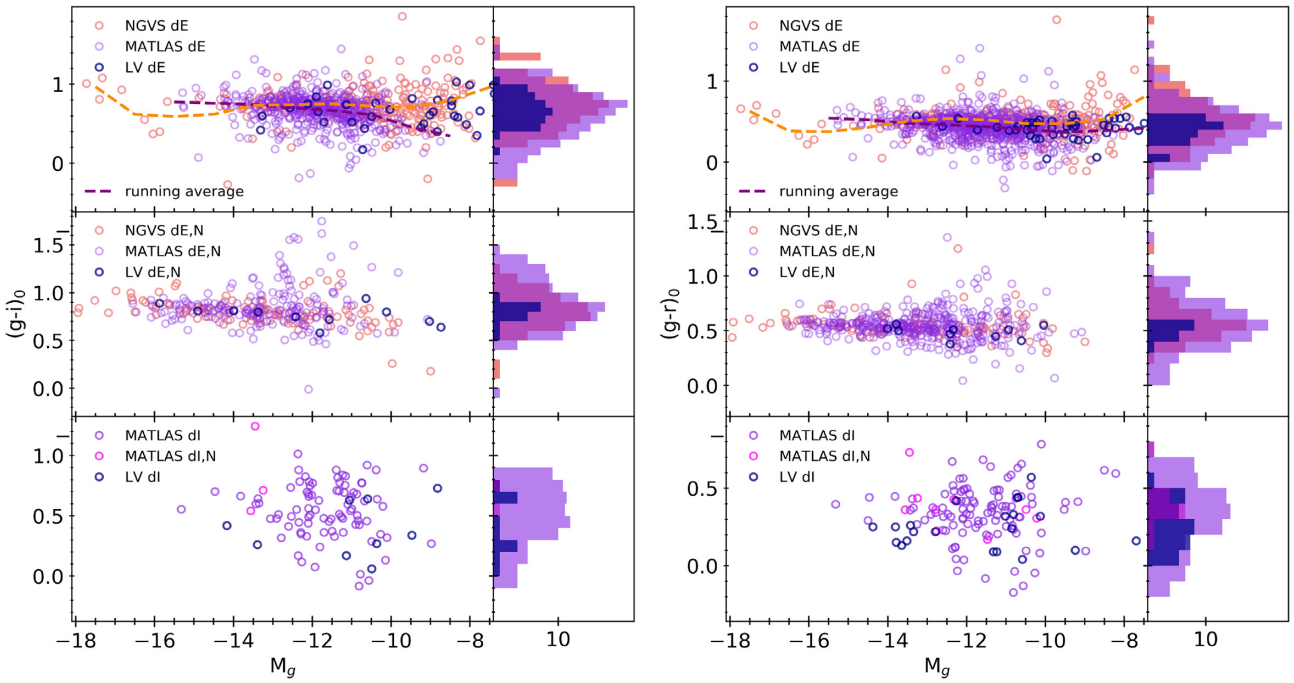

Figure 7. Color–magnitude diagrams of the MATLAS dwarfs (purple) according to the different morphologies compared with the NGVS (orange) and LV (dark blue) dwarfs. Left: $(g-i)_0$ colour comparison. Right: $(g-r)_0$ colour comparison. Dashed lines: running average of the $(g-i)_0$ and $(g-r)_0$ colours for the dE population of MATLAS and NGVS. The colours are corrected for Galactic extinction. The dwarfs are showing similar colours, independently of their local environment.

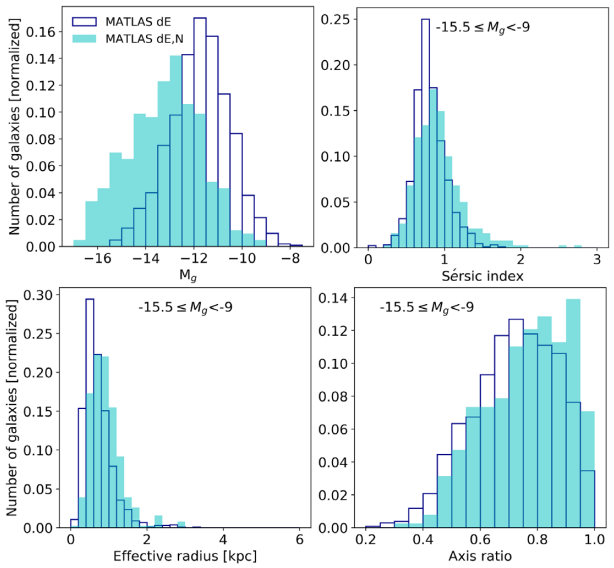

Figure 8. Comparison of distribution of structural properties between MATLAS nucleated and non-nucleated elliptical dwarf galaxies. The histograms are normalized to ensure a better visibility. A shift is visible between the distributions, with the nucleated dwarfs being rounder than non-nucleated dwarfs and less nuclei observed in dwarfs with a Sérsic index < 1 and a R_e < 1 kpc.

by foreground stars is also possible, since they can be confused with unresolved nuclei. Based on the sample of stars observed by the *Gaia* mission (see Appendix A2 for details), we estimated a Galactic star contamination rate of only 0.2 per cent (1/508) in the nucleated sample. We removed this dwarf from the nucleated sample. We note

Table 3. The two-sample KS tests p-values for the bright ($M_g = -17$ to -12) and faint ($M_g = -12$ to -8) dwarf samples as compared to the MATLAS dwarfs properties.

p-values	Sérsic index		Axis ratio		Effective radius	
Sample	Bright	Faint	Bright	Faint	Bright	Faint
NGFS	0.83	0.16	0.40	0.27	0.04	0.26
NGVS	2.40e−3	0.36	0.20	0.55	0.08	2.75e−3
FDS	0.05	0.02	0.02	0.03	0.02	1.07e−4

that another source of contamination can come from background galaxies shining through in the centre.

In this section, we describe how we have extracted the structural and photometric properties of the dwarf nuclei (single or multiple) and present the results.

5.1 Nucleus modelling

To measure the properties of the dwarf nuclei, we used a double profile fit (or multiple profile fit for multiple nuclei) while running GALFIT. The profile fit is composed of a Sérsic fit for the diffuse component and a PSF (unresolved nucleus) or a King profile (slightly extended nucleus) for each of the nuclei (see Fig. 9). If a GALFIT model for the diffuse component was available from the fits with the nucleus masked, we used its parameters as input for GALFIT. When GALFIT encountered a problem finding the position of the nucleus while fitting a PSF or a King profile, we used DAOPHOT to detect it and establish its coordinates.

We visually inspected the results and determined the best models for the nuclei. However, when our visual inspection could not distinguish between the King and PSF models, we used the azimuthally averaged surface brightness profile of both cutout and model images

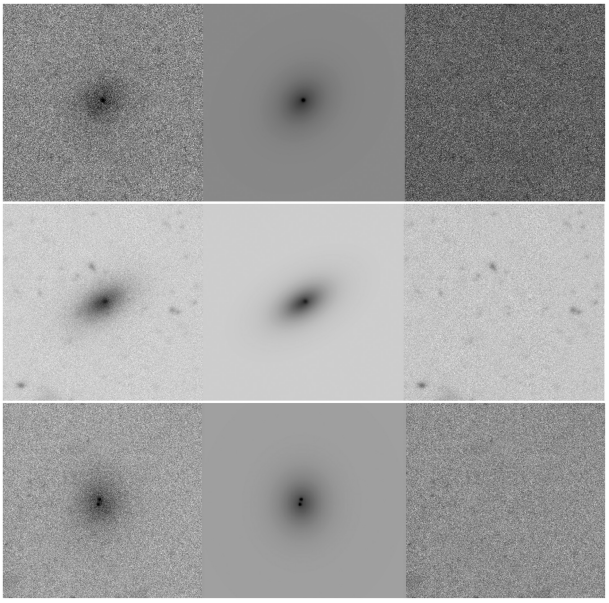

Figure 9. Examples of multiple component fitting. Top: Sérsic + PSF profile. Centre: Sérsic + King profile. Bottom: Sérsic + double PSF profile. The two top rows cutouts are 56 arcsec × 56 arcsec while the bottom row cutouts are 67 arcsec × 67 arcsec. All images have North up and East left.

to identify the best fit. This method, based on Jedrzejewski (1987), fits isophotes and returns the averaged intensity value at each interval of semimajor axis from the centre of the cleaned cut-out image towards the edges. The obtained intensity for each image was then converted to surface brightness after subtracting the background.

Combining both PSF and King profile results, we have GALFIT models for ∼58 per cent of the nuclei.

5.2 Catalogues of NSCs

We used three catalogues of NSCs from cluster dwarfs to compare against the MATLAS nuclei. All the nuclei were modelled by a PSF or a King model. We focus on the Virgo and Fornax clusters by using the nuclei catalogies from the NGVS (Sánchez-Janssen et al. 2019) and NGFS (Ordenes-Briceño et al. 2018), to which we add the catalogue of NSCs located in bright dwarfs and more massive galaxies of the Virgo cluster from Côté et al. (2006). This last study, the ACS Virgo cluster survey (ACSVCS), makes use of the high-resolution data of the Advanced Camera for Surveys (ACS) of the Hubble Space telescope to resolve the NSCs of Virgo elliptical galaxies with $M_g \lesssim -15$. These three catalogues provide us with different information. The NGVS and NGFS both contain the photometric properties, such as M_g or colours, of both the hosts and the nuclei for a sample of dwarfs of similar luminosity to the MATLAS ones. However, only NGFS has information concerning the position of the NSCs as compared to the dwarf photocentre, allowing us to extract an offset value. We note that, similarly to the colour comparison of the dwarfs (see Section 4.3), we restrict the use of the colour information of the NSC to the NGVS, computed using observations from the filters of MegaCam on the CFHT. The ACSVCS, providing the luminosity of both the galaxies and nuclei, allows us to compare the nuclei of faint dwarfs to the ones of bright dEs and more massive ellipticals as well as the photometry extracted from unresolved nuclei observed with a ground-based telescope to the one of resolved nuclei observed with a space telescope in galaxies of similar luminosity.

5.3 Properties of the nuclei

We discuss here several properties of the nuclei based on the GALFIT results. We note that neither the distance of the dwarf or its morphology affect the type of model that best fits the nuclei. All the properties are available in Table 4.

5.3.1 Offset nuclei

In Fig. 10, we present the offset distance separating the nucleus from the photocentre of the dwarf, expressed in arcsecond and fraction of the dwarf R_e, as a function of the dwarf M_g. We indicate the minimum (0.5 arcsec) and maximum (1.61 arcsec) seeing of the MATLAS fields. We compare our nucleated dwarfs to the nucleated dwarfs from NGFS, studied using images of similar quality as MATLAS (average seeing of 1.3 arcsec in the g band, Eigenthaler et al. 2018). The NGFS nuclei have been selected with a maximum offset from the photocentre of 3 arcsec. However, due to the fact that not all nucleated dwarf have been modelled, the maximum offset shown in Fig. 10 is 1.5 arcsec [$0.07R_e$]. The MATLAS nucleated sample show offsets up to 7 arcsec [$0.58R_e$] with a median value of 0.4 arcsec [$0.06R_e$]. Compared to NGFS dwarfs, the MATLAS sample shows similar range of offsets in arcseconds but show more nuclei with a larger offset in terms of fraction of R_e. For both MATLAS and NGFS nucleated samples, the positions of the photocentre and the nucleus is determined by GALFIT while modelling both the galaxy and nucleus. Taking into account the seeing of the MATLAS field images, we can say that we observe offsets nuclei from the photocentre. We have represented the offsets of the MATLAS sample by a colourbar in the top right panel of Fig. 10 as well as in Fig. 11 to look for any effect of the size of the offset on the luminosities and colours of the nuclei. We find no evidence for the nucleus and galaxy to be brighter (or fainter) and bluer (or redder) with a larger offset.

Simulations have shown that dwarf nuclei can be off-centred by up to a few kpc when hosting a massive black hole due to dynamical perturbations (Bellovary et al. 2019). Binggeli, Barazza & Jerjen (2000) have found a typical displacement of 1 arcsec for a sample of 78 dE,N situated in the Virgo cluster. The offset of one of them has later been confirmed by Chung et al. (2019) using the better resolution data from NGVS. They also observed that the offset tends to increase with a decreasing effective surface brightness of the host. A similar result was found in Barazza, Binggeli & Jerjen (2003) for a sample of 16 dE,N also in the Virgo cluster. In the bottom row of Fig. 10 are represented the separation of the MATLAS nuclei as a function of the average surface brightness within R_e, $<\mu_e>$, and the Sérsic index of the dwarf. We display the running average of the offset for different offset ranges. We see a similar trend of the offset increasing in the fainter dwarfs, and moreover, we note an increase of the offset for dwarfs a with fainter center (smaller Sérsic index). Both Binggeli et al. (2000) and Barazza et al. (2003) suggest that this displacement is caused by the oscillation of the nucleus around the centre of the host galaxy due to a less strong gravitational potential (simulations of Miller & Smith 1992; Taga & Iye 1998). We note that this increase of offset could also be due to the fact that it is more difficult to determine the photocentre of objects with lower central surface brightness.

5.3.2 Nuclei colours

The colour of the nuclei can provide valuable insight on their nature and formation scenario. CMRs of the nuclei are visible in Fig. 10 for the $(g-i)_0$ 95 nuclei) and $(g-r)_0$ (162 nuclei) colours. We

Table 4. Properties of the MATLAS nuclei.

ID	Distance (Mpc)		RA (deg)	Dec. (deg)	Offset (arcsec)	m_g	$(g-i)_0$	$(g-r)_0$
(1)	(2)	(3)	(4)	(5)	(6)	(7)	(8)	(9)
MATLAS-8	29.5	–	18.7565	−1.4806	0.62	24.41	0.66	0.42
MATLAS-9	29.5	–	18.7779	−1.2737	1.87	–	–	–
MATLAS-9	29.5	–	18.7788	−1.2745	2.60	–	–	–
MATLAS-10	29.5	–	18.7948	−1.4718	0.50	–	–	–
MATLAS-12	29.5	–	18.8184	−1.5825	0.14	–	–	–
MATLAS-20	30.9	–	19.5842	3.4332	0.58	24.80	0.39	0.36
MATLAS-25	30.9	–	19.8589	3.3598	0.40	24.74	–	0.52
MATLAS-32	35.9	–	20.3636	9.1801	0.56	–	–	–
MATLAS-43	35.9	–	20.6259	8.7853	0.25	–	–	–
MATLAS-44	35.9	–	20.6799	9.4184	0.12	24.83	1.33	0.55
...	...	...	...	...	...	...	...	

Note. The full table is available as supplementary material as well as at CDS. Columns meanings: (1) Dwarf ID; (2) Distance of the assumed host ETG; (3) Distance measurement from [(a)] SDSS DR13 database, [(b)] Poulain et al., in preparation, [(c)] Ann et al. (2015), [(d)] Karachentsev et al. (2013), [(e)] Müller et al. (2021); (4) and (5) Right ascension and declination of the nucleus; (6) Offset distance between the nucleus and the dwarf photocentre; (7) Apparent magnitude in the g band; (8) $g-i$ colour corrected for Galactic extinction; (9) $g-r$ colour corrected for Galactic extinction.

compare our nuclei to NSCs from NGVS and to M31's population of GCs (Peacock et al. 2010). We indicate GALFIT statistical error on the colours. The error is getting larger for an apparent magnitude of the nucleus $m_g \gtrsim 25$ and greater values of the field image seeing. The MATLAS nuclei show a similar range of M_g than NGVS NSCs. When compared to the magnitudes of the GCs around M31, the brightest nuclei in both surveys are ∼4 mag brighter than the brightest GC. Concerning the colours, MATLAS nuclei show a similar distribution of colours to the GC population of similar M_g and a broader range of colours than NGVS NSCs. As already mentioned is the above paragraph, the large range of colour observed for MATLAS is likely not due to the large offsets of the nuclei measured.

When comparing the colours of the dwarf nuclei, we note that we do not distinguish between NSCs and AGNs (or AGNs embedded in NSCs). The low-redshift quasars can show $(g-r)$ colour in the range 0–1.5 (Richards et al. 2002). The identification of the main emission source(s) for the MATLAS nuclei will be investigated in a future publication.

5.4 The nuclei and their dwarf hosts

We now focus our study on the relations between the photometric properties of the nuclei and their dwarf host.

Based on the sample of nuclei successfully modelled, we find a low contribution of the nucleus to the total luminosity of the galaxy (including the nucleus) with a median of 1.7 per cent. We note a contribution above 20 per cent for 6 nuclei, with a maximum contribution of 44.8 per cent. The contribution for each modelled nucleus is visible in Fig. 11. The nuclei of the bright Virgo dwarfs from Binggeli et al. (2000) have a contribution $\lesssim$10 per cent which is consistent with our findings. Despite the large scatter, we see a trend for the contribution to increase towards faint dwarfs, similarly to the nucleus-to-galaxy mass ratio increase towards low-mass dwarfs observed in NGFS (Ordenes-Briceño et al. 2018).

In the Fig. 11, we also show the scaling relation between the magnitude of the nucleus and the magnitude of the host galaxy. We represent in magenta the sample of Virgo elliptical galaxies from ACSVCS, in blue the NGVS nucleated dwarfs and in black the NGFS nucleated dwarfs. The multicolour dots correspond to the MATLAS nucleated dwarfs, whose nuclei have been successfully modelled by a PSF or a King profile. Their colours indicate the offset of the nucleus, with the largest in blue and the smallest in dark red. We can see that the MATLAS dwarfs have similar absolute magnitudes to the NGVS and NGFS dwarfs for both the nuclei and the hosts. A correlation between the magnitude of the nucleus and the magnitude of its host has been found for the ACSVCS elliptical galaxies, and this correlation appears to extend to the NGVS, NGFS, and MATLAS dwarfs.

We plot at the bottom of Fig. 11 the colours of the galaxy as a function of the colours of the nuclei. One can see that there is no clear correlation, as the nuclei are showing both bluer and redder colours than the galaxies.

5.5 Dwarfs with multiple nuclei

The presence of multiple nuclei has been observed in both dwarf and more massive galaxies. In the case of more massive galaxies, the presence of multiple nuclei can be observed during the late stages of the process of galaxy merging. They can occur under the following processes: merging between two galaxies and merging between a galaxy and one of its satellites. The coexistence of AGNs or SMBH coupled to a stellar source (NSC or stellar disc) have been reported in the litterature (examples of dual AGN in Koss et al. 2012; NSC or stellar disc – M31 in Lauer et al. 1993). However, the presence of multiple nuclei in dwarf galaxies has so far been poorly studied. One example is the work of Debattista et al. (2006). They focus on a double nucleated dwarf elliptical galaxy situated in the Virgo cluster and suggest that the nature of this double nucleus is a nuclear disc surrounding a central massive black hole, as seen in M31 or in the low-luminosity galaxy NGC 4486B (Lauer et al. 1996). However, they do not reject the hypothesis of two merging GCs, although they argue it is unlikely. Another example is the study of Pak et al. (2016). They present a double nucleated dwarf lenticular galaxy located in the Ursa Major cluster. They report that this galaxy shows a boxy shape that, in addition to the double nuclei, could be the result of a merger between two galaxies.

Within our sample of nucleated dwarf galaxies, we classified a dwarf galaxy as multinucleated when two to three-point sources of similar magnitude were located close to the galaxy photocentre and appeared brighter than the surrounding point sources. The resulted sample consists of 4 dwarfs with two bright nuclei (our

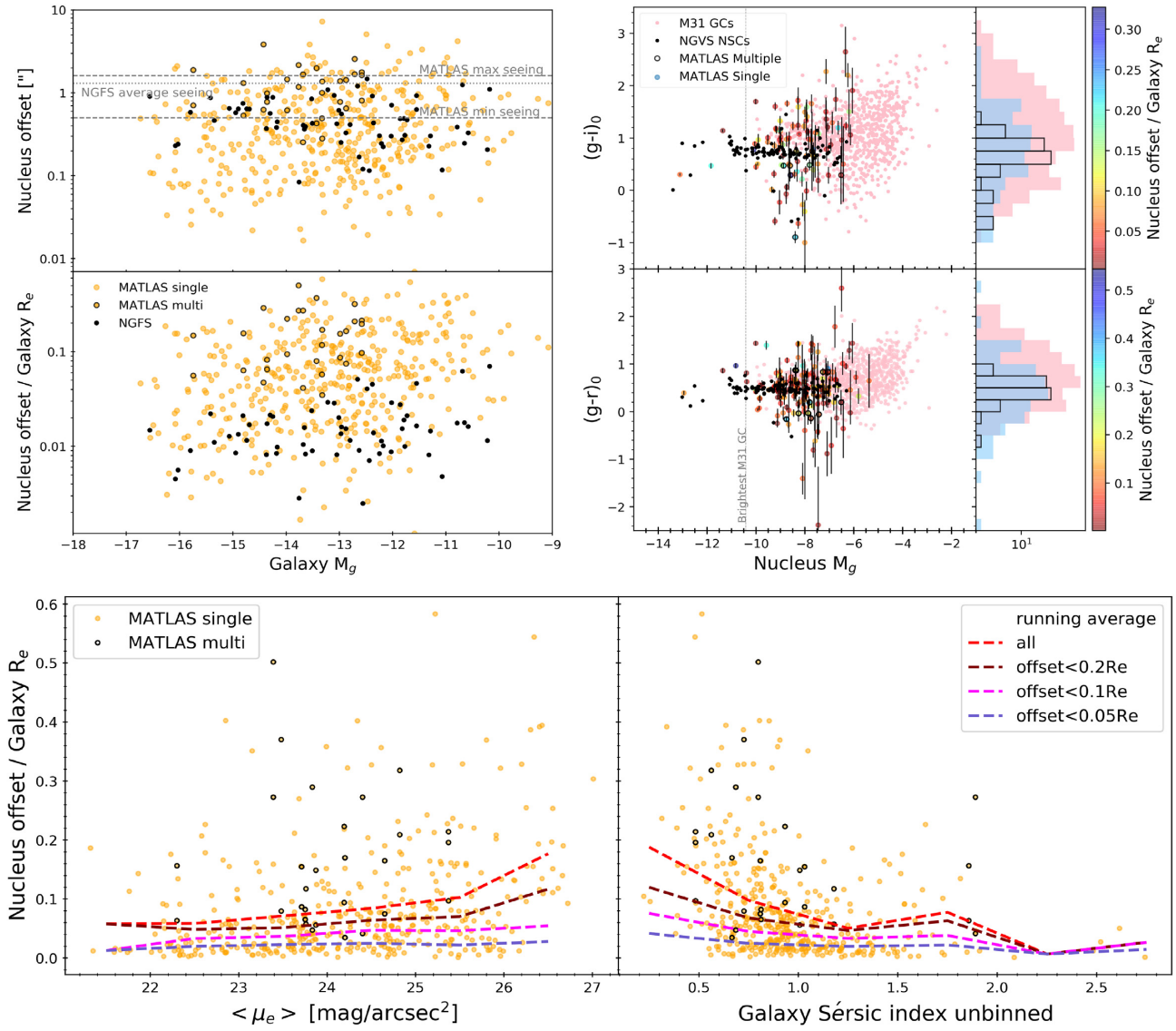

Figure 10. Properties of the MATLAS nuclei. We defined a nucleus as a compact source within ∼0.5 R_e of the dwarf that is the brightest one within one R_e. Top left panel: Estimated offset between the photocentre of the host galaxy and the nucleus in arcsecond (top) and fraction of the dwarf R_e (bottom) as a function of the absolute magnitude M_g of the dwarf. Yellow dots: MATLAS dwarfs with a single nucleus. Circled yellow dots: MATLAS dwarfs with mutiple nuclei. Black dots: nucleated dwarfs in NGFS. Dashed lines: minimum and maximum seeing of the MATLAS field g-band images. Dotted line: average seeing of NGFS g-band images. Top right panel: Colour–magnitude diagrams of the nuclei compared to M31 globular clusters and NGVS dwarfs nuclei. Top: $(g-i)_0$ colour comparison. Bottom: $(g-r)_0$ colour comparison. Dashed line: M_g of the brightest M31 GC. Colourbars: offset of the nucleus from the photocentre expressed in fraction of R_e of the galaxy host. Error bars: GALFIT statistical errors on the colours. A similar range of M_g is observed for the MATLAS nuclei and NGVS NSCs, while the MATLAS nuclei show similar $(g-i)$ and $(g-r)$ colours than M31 GCs. Bottom panel: Nucleus–photocentre separation expressed in fraction of the dwarf R_e as a function of the average surface brightness within R_e in the g band (left) and the Sérsic index of the dwarf (right). Yellow dots: MATLAS dwarfs with a single nucleus. Circled yellow dots: MATLAS dwarfs with multiple nuclei. Dashed lines: running average of the offset for different offset ranges. A trend of the separation increasing in the fainter dwarfs with fainter centres is visible.

best candidates), 11 with a two faint nuclei, and one with a three faint nuclei. As discussed above in Section 5.1, for those galaxies, a multiple component profile (a PSF or King model for each nucleus in addition to a Sérsic model) was used for GALFIT. In Fig. 9, we show a GALFIT modelling result for a double nucleated dwarf using a Sérsic profile coupled to a PSF for both nuclei. We obtained a GALFIT model of both the galaxy and its nuclei for 8 of the 15 double nucleated as well as for the triple nucleated and a GALFIT model of the galaxy alone for 3 double nucleated. The multiple nucleated successfully modelled are represented with black edged dots in Figs 10 and 11. As for the single nucleated, the magnitude of the nuclei seems to be correlated with the one of the host galaxies. The nuclei off-centre distances also spans the same range of amplitudes and galaxy magnitudes as for the single nucleated.

As tidal features and isophotal distortions (boxy) are associated with merger remnants, we have looked for these features in our multinucleated dwarf sample using their corresponding field images. None of our multinucleated dwarfs have boxy isophotes. However, we find tidal features for one candidate. This galaxy shows a tidal tail that indicates a late stage merger between two dwarf galaxies and could provide as well an explanation for the presence of the two bright nuclei.

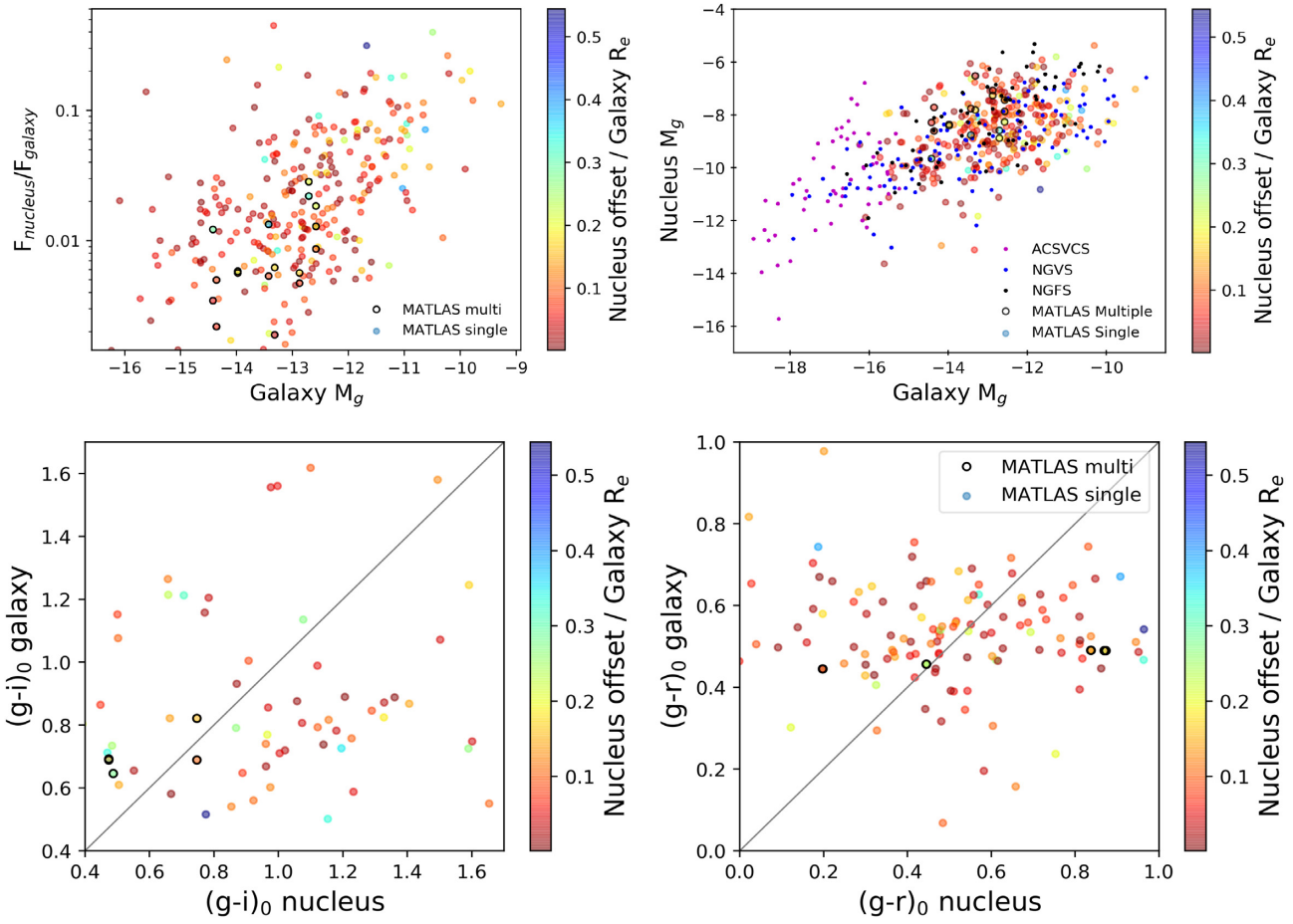

Figure 11. Relations between the nucleus (as defined in Fig. 10) and the dwarf host. Top left: Contribution of the nucleus to the total luminosity of the galaxy per M_g. Top right: The absolute magnitude of nucleus as a function of the absolute magnitude the host galaxy for NGFS (black dots) and NGVS (blue dots) dwarf galaxies, as well as ACSVCS elliptical galaxies (magenta dots) and the MATLAS dwarfs (open black dots: multiple nuclei, multicolour dots: single nucleus). The MATLAS, NGFS, and NGVS dwarfs are showing similar absolute magnitudes for both the nuclei and galaxies. Moreover, the correlation between the magnitude of the nucleus and the magnitude of its host found for the elliptical galaxies appears to extend to the dwarfs. Bottom: Colour–colour diagrams of the galaxy as a function of the nucleus. Left: $(g-i)_0$ colour comparison. Right: $(g-r)_0$ colour comparison. No tendency for the nuclei to be bluer or redder than the galaxy is observed. Colourbars: offset of the nucleus from the photocentre expressed in fraction of R_e of the galaxy host.

6 ENVIRONMENTAL ROLE ON THE FORMATION SCENARIOS

We have presented the structural and photometric properties of the MATLAS dwarfs as well as of their nuclei. We have compared these results with the findings in different density environments. We now discuss the implications in terms of formation scenarios and evolution of the dwarf galaxies and their central compact nuclei.

6.1 Dwarfs formation scenario, evolution, and environment

In this section, we analyse the different findings regarding the MATLAS dwarfs population to estimate the effect of the environment on the formation and evolution of the dwarf galaxies. We know from Habas et al. (2020) that we observe a morphologydensity relation for the MATLAS dwarfs with a tendency for the dIs to be located in lower local density environments than dEs and for the nucleated population to be situated in higher local density environments than non-nucleated dwarfs. This relation is also observed in higher density environments. The dIs are preferentially found in the outskirts of clusters, the LG and nearby groups in the LV (Ferguson & Sandage 1990; Skillman, Côté & Miller 2003; Côté et al. 2009; McConnachie 2012) and the nucleated are in majority situated close to the centre of the clusters (Ferguson & Sandage 1989). This morphology–density relation, coupled to the fact that we find a difference of structural properties between the dE and dE,N populations, implies that the local environment plays a role in shaping dwarf galaxies.

Several formation scenarios of the dEs, based on external processes, were put forward according to the environment. In the LG, simulations show that tidal stripping is needed to recover the observed properties of the dwarfs (Mayer et al. 2001; Sawala, Scannapieco & White 2012). In clusters, the harassment and ram-pressure stripping of late-type galaxies during their infall are favored to explain the red colours of the elliptical dwarfs (Mastropietro et al. 2005; Boselli et al. 2008; Steyrleithner, Hensler & Boselli 2020). However, as this work shows, the similarities observed between the photometric and structural properties of the dwarfs located in vastly different environments imply that they are likely drawn from the same population and thus have a similar formation scenario. Murali (2000) shows that ram-pressure stripping is not efficient to form the Milky-Way satellites. The finding of isolated rotating dEs in the field (with a distance to a massive neighbour $>$ 1 Mpc) at distances between 27 and 83 Mpc by Janz et al. (2017) indicate that

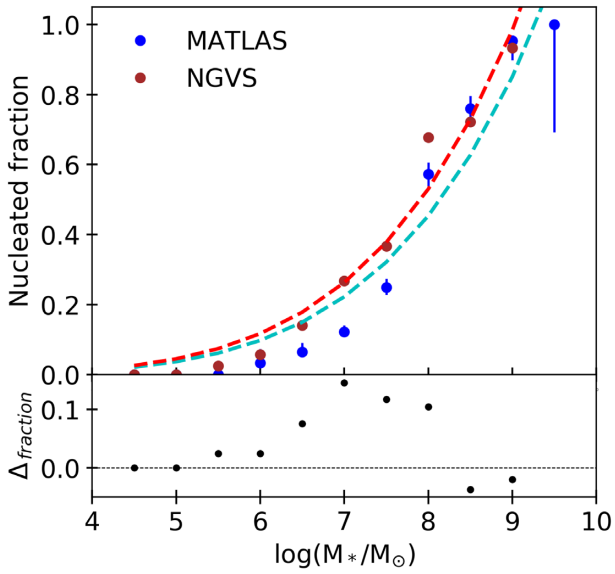

Figure 12. Nucleated fraction as a function of the stellar mass. Blue dots: MATLAS dwarfs. Red dots: NGVS dwarfs. Dashed lines: best power-law fit. Error bars: 1σ binomial confidence intervals. The nucleated fraction of the MATLAS sample falls systematically below the NGVS sample.

they are not necessarily the result of harassment and ram-pressure stripping in clusters. In the low-density environment of MATLAS, we find a dE population with, on average, colours as red as the dEs in clusters, which also implies that dEs are not uniquely the product of morphological transformation due to ram-pressure stripping and galaxy harassment in high-density environments. This result also suggests that some, if not all, dEs in the cluster environment may have formed prior to infall.

6.2 Formation scenario of the compact central nuclei

In the following, we discuss the results concerning the MATLAS nucleated dwarfs sample and their nuclei in the context of formation scenario of the nucleus. Currently, two main formation scenarios are under debate: the *in situ* formation by gas infall and the migration followed by the merging of GCs towards the centre. After this discussion, we will also examine the hypothesis of the nuclei as being ultracompact dwarfs (UCDs) progenitors.

6.2.1 Nucleated fraction mass dependence

We investigate the nucleated dwarf fraction as a function of the stellar mass as in Sánchez-Janssen et al. (2019). We estimated the stellar masses of our MATLAS dwarfs using the stellar mass-to-light ratios from Bell et al. (2003). We chose to compute the stellar masses from the $g-r$ colour, as we have a larger number of modelled galaxies than with the $g-i$ colour. The nucleated fraction was calculated per bin of 0.5 in stellar mass. The result can be seen in Fig. 12. The MATLAS sample is shown in blue and the NGVS sample is in red. We have fitted a power-law function for both samples and the best fits are shown with the dashed lines. Sánchez-Janssen et al. (2019) found that the nucleated fraction increases with stellar mass, which we also observe in the low-to-moderate density environments of the MATLAS sample. As well as this mass dependence, Sánchez-Janssen et al. (2019) report a possible effect of the environment on the nucleated fraction. They compared their fraction to the ones of the LG, the Coma cluster, and Fornax cluster, considering the clusters core populations (within $\sim$0.25 $R_{\rm vir}$). Comparing to the Virgo and Fornax clusters that show an almost identical fraction for a similar mass bin, they found that the fraction for Coma is systematically larger while the fraction for the LG is smaller. Similarly, for the MATLAS sample, we observe that the fraction of nucleated is lower than the one of NGVS at a given stellar mass. Moreover, while we observe dwarfs with stellar masses as low as $\log(M_*/{\rm M}_\odot) = 5.17$ and 4.8 for the MATLAS and NGVS, respectively, the value of the stellar mass from which the fraction becomes non-null seems to be higher towards lower density environments, with a value of $M_* \sim 5\times10^5\,{\rm M}_\odot$ for NGVS and $M_* \sim 1\times10^6\,{\rm M}_\odot$ for MATLAS. Zanatta et al. (2021) and Carlsten et al. (2021) report a similar effect of the environment on the nucleated fraction of dwarfs located in groups from the LV. As mentioned in Sánchez-Janssen et al. (2019), these results suggest that nuclei in low-to-moderate density environments tend to form in lower quantities than in higher density environments.

One possible explanation for this environmental difference could be the effect of tidal perturbations on the dwarfs. Oh & Lin (2000) made use of numerical simulations to test the migration scenario in cluster dwarfs. They found that dwarfs located in the outskirts of clusters experience tidal disruption that extends GCs orbits and lengthens the dynamical friction time-scales, making the formation of nuclei difficult. While in the core cluster, the tidal perturbations compress and protect the dwarf integrity, leading to the formation of nuclei by the migration and merging of the GCs.

To test this hypothesis, we compare the nucleated fraction of dwarfs with M_* in the range 10^7–$10^9\,{\rm M}_\odot$ located in different environments: cluster core, cluster outskirt, group, group outskirt, and field. Sánchez-Janssen et al. (2019) found a nucleated fraction of 77, 53, and 56 per cent in the cluster core of Coma, Virgo, and Fornax, respectively, and a fraction of 29 per cent in the LG. We compute a fraction of 51 per cent for the MATLAS dwarfs located within the projected virial radii of a group,[3] and 39 per cent for the MATLAS dwarfs located beyond. We use the FDS sample to estimate the fraction of nucleated in and outside the core ($\sim$0.25$R_{\rm vir}$) of the Fornax cluster. We find a nucleated fraction of 56 per cent in the core, as Sánchez-Janssen et al. (2019), and 19 per cent outside. The results are consistent with what we would expect from the effects of tidal perturbations. The dwarfs in the outskirts of Fornax and in the LG suffer from tidal disruption, leading to a fraction smaller than in cluster core. The MATLAS dwarfs are found in groups with masses in the range $\sim 3\times10^8$–$9\times10^{13}\,{\rm M}_\odot$, reaching masses similar to the Fornax cluster and explaining the obtained fraction, similar to the Fornax core but still slightly smaller due to the tidally disrupted dwarfs found in less massive groups. In fact, we observe a decreasing nucleated fraction towards less massive groups, with 48 per cent for dwarfs in groups with a mass below 5×10^{12}, 51 per cent for a mass range 5×10^{12}–10^{13} and 52 per cent above 10^{13}. While the MATLAS dwarfs located in lower density environments, especially in groups outskirts, are more likely to undergo tidal disruption, leading to a smaller nucleated fraction.

6.2.2 Relations between the nuclei and their host

Some studies have put forward a mass dependence for the formation scenario of the nuclei with a turnover at a stellar mass of $M_* \sim 10^9$

[3]Considering the galaxy groups located at distances <50 Mpc in the catalogue from Kourkchi & Tully (2017), with virial radii adapted using $H_0 = 70$ km s^{-1} Mpc^{-1}.

$M_{\odot}$. They suggest that the *in situ* process dominates at the high galaxy mass regime while nuclei of low-mass galaxies are more likely to be formed from GCs migration and merging (Turner et al. 2012; Fahrion et al. 2021). The observed correlation between the nucleus and galaxy magnitude for both dwarfs and more massive ellipticals is consistent with both formation scenarios (Lotz, Miller & Ferguson 2004). Coupled to the wide range of relative colours of nuclei and the host galaxies, this argues that the galaxy and the nucleus have formed together and then followed a different evolution (Grant, Kuipers & Phillipps 2005). We can link this result to the mass dependence of the nucleated fraction and suggest that, similarly to Ordenes-Briceño et al. (2018) and Sánchez-Janssen et al. (2019), the NSCs can form together with the galaxy but get more easily disrupted in lower mass dwarfs.

In the context of the migration scenario being dominant in low-mass galaxies, observing dwarfs nuclei with colours similar to GCs as well as dwarfs showing multiple nuclei suggest that these nuclei may form from GCs migration and merging. However, we cannot reject a possible contamination of a small fraction of the nuclei sample by GC, and we note that the presence of multiple nuclei can also be explained by nucleated dwarf galaxies merging, when coupled to signs of merging process such as tidal tails.

Another formation scenario of the dwarfs nuclei, combining both the *in situ* and migration ones, is the wet migration scenario. The presence or absence of clusters merger in this scenario affects the star formation activity of the NSC, with its quenching after a merger. This scenario can explain the presence in the MATLAS sample of blue nuclei, possibly off-centred, as well as the observation of double nuclei. We note that Paudel & Yoon (2020) found off-centred nuclei-like star-forming regions in red dEs whose properties are consistent with the wet migration scenario.

Our observations also are consistent with the findings of spectroscopic studies. While NSC and galaxy photometry give an estimate of the age and metallicity of their stellar population, the spectroscopic studies allow one to measure these quantities and compute the star formation history. Comparative studies between dE nuclei and their host galactic main body have revealed mixed results. Paudel, Lisker & Kuntschner (2011) show that the nuclei are significantly younger and metal-rich than the host galaxies, while Fahrion et al. (2020) and Johnston et al. (2020) show that nuclei have lower metallicities than their host galaxies. On the other hand, Spengler et al. (2017) show no clear differences in age or metallicity of the dE nuclei with their host galaxies. Due to its large size, low surface brightness and numerous GCs, the dwarf MATLAS-2019 was particularly focused in recent studies. Forbes et al. (2019) suggest that one of the central bright GCs might be an NSC. Considering this assumption and the results of the spectroscopic study of Müller et al. (2020), these bright star clusters (named GC5 and GC6 in that study) show no significant difference in metallicity as compared to the host galaxy, which would be in agreement with the results of Spengler et al. (2017), such as the absence of relation between the nuclei and hosts colours found in the MATLAS sample.

6.2.3 *MATLAS nuclei as UCD progenitors*

Having discussed the formation scenario of the nuclei, we now focus on one of the possible formation scenarios of UCDs that suggests that they are the remnants of tidally disrupted nucleated dwarf galaxies (Bassino, Muzzio & Rabolli 1994; Bekki, Couch & Drinkwater 2001; Voggel, Hilker & Richtler 2016). In Fig. 13, we show the distribution of M_g of the nuclei modelled by both a King profile or a PSF that we compare to UCDs located in the Virgo cluster (Liu et al. 2020) and to GCs from M31 (Peacock et al. 2010). We can see that the distribution of MATLAS nuclei magnitudes falls in between the UCDs and GCs. As UCDs have absolute magnitudes that overlap the distribution of the bright dwarfs nuclei (as well as the brightest GCs), this result suggests that some of the MATLAS nuclei may be progenitors of UCDs. However, due to the lack of information concerning the size of the MATLAS nuclei, we cannot test the robustness of this result.

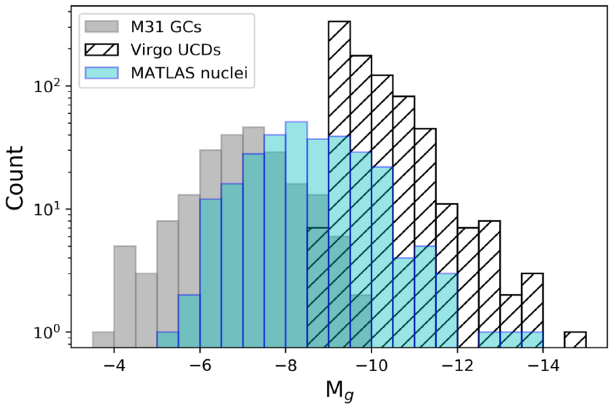

Figure 13. Comparison of M_g between MATLAS nuclei, M31 GCs and UCDs from the Virgo cluster. The overlapping of UCDs absolute magnitudes with some of the dwarfs nuclei suggests that some of the MATLAS nuclei may be progenitors of UCDs. The counts are displayed in log scale to ensure a better visibility.

7 CONCLUSION

We have studied the structure and morphology of a sample of 2210 dwarf galaxies located in the low-to-moderate density environments of the MATLAS fields. We visually identified a sample of 508 nucleated galaxies that includes a sub-sample of 16 dwarfs showing possible multiple nuclei. With the use of the software GALFIT, we have modelled the dwarf galaxies with a Sérsic profile and their compact central nuclei with a PSF or a King profile and obtain a reliable modelling for 1589 galaxies (1022 dEs, 142 dIs, 415 dE,N, and 10 dI,N), among them 292 nuclei. We provided the catalogues of structural and photometric properties of the MATLAS dwarfs as well as the nuclei properties. We have compared the structural and photometric properties of the dwarfs with galaxies from the LG, LV as well as from the Virgo and Fornax clusters. We report the following results:

(i) Considering dwarfs in the same range of M_g, the MATLAS and clusters dwarfs are showing similar range of R_e, axis-ratio, and Sérsic index while the LV and LG dwarfs are showing a similar range of R_e to the MATLAS dwarfs.

(ii) Two-sample KS tests, using a significance level $\alpha = 0.05$, have shown that we cannot reject the hypothesis, for most of the structural properties of bright and faint MATLAS and clusters core dwarfs, that they are drawn from the same population.

(iii) The MATLAS dwarfs show similar $(g-i)_0$ and $(g-r)_0$ colours as compared to the dwarfs located in the Virgo cluster and in the LV, meaning that we find, on average, that dEs are as red in low-to-moderate density environments as they are in the cluster environment.

(iv) As observed in clusters, the MATLAS nucleated dwarfs are brighter and, for similar luminosities, are rounder than the non-nucleated dwarfs. We also observe fewer nuclei in dwarfs with a

faint centre (i.e. a Sérsic index < 1) and a small size (i.e. a $R_e <$ 1 kpc).

We defined a nucleus as a compact source within $\sim 0.5 R_e$ of the dwarf that is the brightest one within one R_e. Focusing on the properties of the nuclei in the nucleated sample, we find the following results:

(i) We observe a systematic displacement of the nuclei that tend to increase towards dwarfs with low $<\mu_e>$ and low Sérsic index. This can be caused by the oscillation of the nucleus around the centre of the host galaxy due to a less strong gravitational potential or by an increase of the uncertainty in the determination of the photocentre.

(ii) The MATLAS, NGFS, and NGVS nuclei show a similar range of M_g. The MATLAS nuclei have ranges of $g - i$ and $g - r$ colours similar to M31 GCs.

(iii) The larger range of colours observed in the MATLAS sample, as compared to the NGVS one, is likely not due to the large offsets of the MATLAS nuclei measured.

(iv) We find a low contribution of the nucleus to the total luminosity of the galaxy with a median of 1.7 per cent, consistent to the observed contribution of bright dwarf galaxies in the Virgo cluster, and a trend for the contribution of the nucleus to increase towards faint dwarfs.

(v) Our findings of the correlation between the nucleus and galaxy magnitude and the absence of relation between the colours of nuclei and their host galaxies is consistent with the scenario of galaxies and nuclei forming together but followed by a different evolution.

(vi) We find an increasing nucleated fraction towards high stellar masses. For a similar mass, this fraction is systematically smaller than the one of the NGVS sample, suggesting that nuclei in low-to-moderate density environments tend to form in lower quantities than in higher density environments. This difference could be explained by tidal perturbations encountered in moderate density environments.

(vii) The nuclei colours, offsets, and the observations of possible multiple nuclei are consistent with the migration and wet migration formation scenarios.

(viii) As the bright MATLAS nuclei ($M_g < -8.5$) show similar M_g to UCDs from the Virgo cluster, they may be progenitors of UCDs.

Multiband ground-based imaging under good seeing conditions are a powerful probe to simultaneously study nuclei and their host galaxies. Ultimately, we need spectroscopy to confirm their association and get the information of age and metallicity to study their formation paths.

ACKNOWLEDGEMENTS

We thank the referee for the constructive report that helped to improve this manuscript. Based on observations obtained with MegaPrime/MegaCam, a joint project of CFHT and CEA/IRFU, at the Canada–France–Hawaii Telescope (CFHT) which is operated by the National Research Council (NRC) of Canada, the Institut National des Science de l'Univers of the Centre National de la Recherche Scientifique (CNRS) of France, and the University of Hawaii. This work is based in part on data products produced at Terapix available at the Canadian Astronomy Data Centre as part of the Canada–France–Hawaii Telescope Legacy Survey, a collaborative project of NRC and CNRS. MP acknowledges the Vice Rector for Research of the University of Innsbruck for the granted scholarship. SP acknowledges support from the New Researcher Program (Shinjin grant No. 2019R1C1C1009600) through the National Research Foundation of Korea. SL acknowledges the support from the Sejong Science Fellowship Program through the National Research Foundation of Korea (NRF-2021R1C1C2006790). MB acknowledges the support from the Polish National Science Centre under the grant 2017/26/D/ST9/00449. This work has made use of data from the European Space Agency (ESA) mission *Gaia* (https://www.cosmos.esa.int/gaia), processed by the *Gaia* Data Processing and Analysis Consortium (DPAC, https://www.cosmos.esa.int/web/gaia/dpac/consortium). Funding for the DPAC has been provided by national institutions, in particular the institutions participating in the *Gaia* Multilateral Agreement.

DATA AVAILABILITY

The data underlying this article are available at the CDS.

REFERENCES

Adami C. et al., 2006, A&A, 459, 679
Aguerri J. A. L., González-García A. C., 2009, A&A, 494, 891
Ann H. B., Seo M., Ha D. K., 2015, ApJS, 217, 27
Antonini F., Capuzzo-Dolcetta R., Mastrobuono-Battisti A., Merritt D., 2012, ApJ, 750, 111
Arenou F. et al., 2018, A&A, 616, A17
Barazza F. D., Binggeli B., Jerjen H., 2003, A&A, 407, 121
Bassino L. P., Muzzio J. C., Rabolli M., 1994, ApJ, 431, 634
Bekki K., 2007, Publ. Astron. Soc. Aust., 24, 77
Bekki K., Couch W. J., Drinkwater M. J., 2001, ApJ, 552, L105
Bell E. F., McIntosh D. H., Katz N., Weinberg M. D., 2003, ApJS, 149, 289
Bell E. F. et al., 2004, ApJ, 608, 752
Bellazzini M. et al., 2008, AJ, 136, 1147
Bellovary J. M., Cleary C. E., Munshi F., Tremmel M., Christensen C. R., Brooks A., Quinn T. R., 2019, MNRAS, 482, 2913
Bertin E., 2011, in Evans I. N., Accomazzi A., Mink D. J., Rots A. H., eds, ASP Conf. Ser. Vol. 442, Astronomical Data Analysis Software and Systems XX. Astron. Soc. Pac., San Francisco, p. 435
Bertin E., Arnouts S., 1996, A&AS, 117, 393
Binggeli B., Barazza F., Jerjen H., 2000, A&A, 359, 447
Boselli A., Boissier S., Cortese L., Gavazzi G., 2008, ApJ, 674, 742
Butler D. J., Martínez-Delgado D., 2005, AJ, 129, 2217
Cappellari M. et al., 2011, MNRAS, 413, 813
Carlsten S. G., Greco J. P., Beaton R. L., Greene J. E., 2020, ApJ, 891, 144
Carlsten S. G., Greene J. E., Beaton R. L., Greco J. P., 2021, preprint(arXiv:2105.03440)
Chung J., Rey S.-C., Sung E.-C., Kim S., Lee Y., Lee W., 2019, ApJ, 879, 97
Côté P. et al., 2006, ApJS, 165, 57
Côté S., Draginda A., Skillman E. D., Miller B. W., 2009, AJ, 138, 1037
De Rijcke S., Prugniel P., Simien F., Dejonghe H., 2006, MNRAS, 369, 1321
Debattista V. P., Ferreras I., Pasquali A., Seth A., Rijcke S. D., Morelli L., 2006, ApJ, 651, L97
Dekel A., Silk J., 1986, ApJ, 303, 39
den Brok M. et al., 2014, MNRAS, 445, 2385
den Brok M. et al., 2015, ApJ, 809, 101
Draper P. W., Gray N., Berry D. S., Taylor M., 2014, Astrophysics Source Code Library, record ascl:1403.024
Duc P.-A. et al., 2014, MNRAS, 446, 120
Dunn J. M., 2015, MNRAS, 453, 1799
Eigenthaler P. et al., 2018, ApJ, 855, 142
Fahrion K. et al., 2020, A&A, 634, A53
Fahrion K. et al., 2021, A&A, 650, A137
Ferguson H. C., Binggeli B., 1994, A&AR, 6, 67
Ferguson H. C., Sandage A., 1989, ApJ, 346, L53
Ferguson H. C., Sandage A., 1990, in Hollenbach D. J., Thronson Harley A. J., eds, NASA Conference Publication, Vol. 3084. National Aeronautics and Space Administration, Washington, DC, p. 281
Ferguson H. C., Sandage A., 1991, AJ, 101, 765
Ferrarese L. et al., 2012, ApJS, 200, 4

Ferrarese L. et al., 2020, ApJ, 890, 128
Forbes D. A., Gannon J., Couch W. J., Iodice E., Spavone M., Cantiello M., Napolitano N., Schipani P., 2019, A&A, 626, A66
Gaia Collaboration, 2016, A&A, 595, A1
Gaia Collaboration, 2018, A&A, 616, A1
Geha M., Blanton M. R., Yan R., Tinker J. L., 2012, ApJ, 757, 85
Georgiev I. Y., Hilker M., Puzia T. H., Goudfrooij P., Baumgardt H., 2009, MNRAS, 396, 1075
Georgiev I. Y., Puzia T. H., Goudfrooij P., Hilker M., 2010, MNRAS, 406, 1967
Graham A. W., Driver S. P., 2005, Publ. Astron. Soc. Aust., 22, 118
Grant N. I., Kuipers J. A., Phillipps S., 2005, MNRAS, 363, 1019
Grebel E. K., 2001, in de Boer K. S., Dettmar R.-J., Klein U., eds, Dwarf Galaxies and Their Environment. Shaker Verlag, Bonn, p. 45
Grebel E. K., 2004, in McWilliam A., Rauch M., eds, Origin and Evolution of the Elements. Cambridge Univ. Press, Cambridge, p. 234
Guillard N., Emsellem E., Renaud F., 2016, MNRAS, 461, 3620
Habas R. et al., 2020, MNRAS, 491, 1901
Haines C. P., Gargiulo A., Merluzzi P., 2008, MNRAS, 385, 1201
Harris W. E., 2010, preprint(arXiv:1012.3224)
Harris W. E., van den Bergh S., 1981, AJ, 86, 1627
Harris W. E., Harris G. L. H., Alessi M., 2013, ApJ, 772, 82
Ho L. C., Li Z.-Y., Barth A. J., Seigar M. S., Peng C. Y., 2011, ApJS, 197, 21
Janz J., Penny S. J., Graham A. W., Forbes D. A., Davies R. L., 2017, MNRAS, 468, 2850
Jedrzejewski R. I., 1987, MNRAS, 226, 747
Johnston E. J. et al., 2020, MNRAS, 495, 2247
Jordán A. et al., 2006, ApJ, 651, L25
Karachentsev I. D., Makarov D. I., Kaisina E. I., 2013, AJ, 145, 101
Kaviraj S., Martin G., Silk J., 2019, MNRAS, 489, L12
Kent S. M., 1987, AJ, 94, 306
Koss M., Mushotzky R., Treister E., Veilleux S., Vasudevan R., Trippe M., 2012, ApJ, 746, L22
Kourkchi E., Tully R. B., 2017, ApJ, 843, 16
Lauer T. R. et al., 1993, AJ, 106, 1436
Lauer T. R. et al., 1996, ApJ, 471, L79
Lauer T. R., Faber S. M., Ajhar E. A., Grillmair C. J., Scowen P. A., 1998, AJ, 116, 2263
Lim S. et al., 2020, ApJ, 899, 69
Lindegren L. et al., 2018, A&A, 616, A2
Liu C. et al., 2020, ApJS, 250, 17
Loose H. H., Kruegel E., Tutukov A., 1982, A&A, 105, 342
Lotz J. M., Miller B. W., Ferguson H. C., 2004, ApJ, 613, 262
Marleau F. R., Clancy D., Bianconi M., 2013, MNRAS, 435, 3085
Marleau F. R., Clancy D., Habas R., Bianconi M., 2017, A&A, 602, A28
Mastropietro C., Moore B., Mayer L., Debattista V. P., Piffaretti R., Stadel J., 2005, MNRAS, 364, 607
Mateo M. L., 1998, ARA&A, 36, 435
Mayer L., Governato F., Colpi M., Moore B., Quinn T., Wadsley J., Stadel J., Lake G., 2001, ApJ, 547, L123
McConnachie A. W., 2012, AJ, 144, 4
Mezcua M., Domínguez Sánchez H., 2020, ApJ, 898, L30
Miller R. H., Smith B. F., 1992, ApJ, 393, 508
Misgeld I., Mieske S., Hilker M., 2008, A&A, 486, 697
Mistani P. A. et al., 2016, MNRAS, 455, 2323
Molina M., Reines A. E., Greene J. E., Darling J., Condon J. J., 2021, ApJ, 910, 5
Monaco L., Bellazzini M., Ferraro F. R., Pancino E., 2005, MNRAS, 356, 1396
Moore B., Katz N., Lake G., Dressler A., Oemler A., 1996, Nature, 379, 613
Müller O., Jerjen H., Binggeli B., 2017, A&A, 597, A7
Müller O., Jerjen H., Binggeli B., 2018, A&A, 615, A105
Müller O. et al., 2020, A&A, 640, A106
Müller O. et al., 2021, preprint(arXiv:2101.10659)
Murali C., 2000, ApJ, 529, L81
Neumayer N., Seth A., Böker T., 2020, A&AR, 28, 4
Oh K. S., Lin D. N. C., 2000, ApJ, 543, 620
Ordenes-Briceño Y. et al., 2018, ApJ, 860, 4
Pak M., Paudel S., Lee Y., Kim S. C., 2016, AJ, 151, 141
Pasetto S., Chiosi C., Carraro G., 2003, A&A, 405, 931
Paudel S., Yoon S.-J., 2020, ApJ, 898, L47
Paudel S., Lisker T., Kuntschner H., 2011, MNRAS, 413, 1764
Peacock M. B., Maccarone T. J., Knigge C., Kundu A., Waters C. Z., Zepf S. E., Zurek D. R., 2010, MNRAS, 402, 803
Peng C. Y., Ho L. C., Impey C. D., Rix H.-W., 2010, AJ, 139, 2097
Richards G. T. et al., 2002, AJ, 123, 2945
Sánchez-Janssen R. et al., 2016, ApJ, 820, 69
Sánchez-Janssen R. et al., 2019, ApJ, 878, 18
Sawala T., Scannapieco C., Maio U., White S., 2010, MNRAS, 402, 1599
Sawala T., Scannapieco C., White S., 2012, MNRAS, 420, 1714
Schlafly E. F., Finkbeiner D. P., 2011, ApJ, 737, 103
Secker J., 1995, PASP, 107, 496
Sérsic J. L., 1963, BAAA, 6, 41
Sharina M. E. et al., 2008, MNRAS, 384, 1544
Sills A., Dalessandro E., Cadelano M., Alfaro-Cuello M., Kruijssen J. M. D., 2019, MNRAS, 490, L67
Simon J. D., 2019, ARA&A, 57, 375
Skillman E. D., Côté S., Miller B. W., 2003, AJ, 125, 593
Spengler C. et al., 2017, ApJ, 849, 55
Stetson P. B., 1987, PASP, 99, 191
Steyrleithner P., Hensler G., Boselli A., 2020, MNRAS, 494, 1114
Taga M., Iye M., 1998, MNRAS, 299, 111
Tremaine S. D., Ostriker J. P., Spitzer L. J., 1975, ApJ, 196, 407
Turner M. L., Côté P., Ferrarese L., Jordán A., Blakeslee J. P., Mei S., Peng E. W., West M. J., 2012, ApJS, 203, 5
Valcke S., de Rijcke S., Dejonghe H., 2008, MNRAS, 389, 1111
van den Bergh S., 1960, ApJ, 131, 215
van Dokkum P. G., Abraham R., Merritt A., Zhang J., Geha M., Conroy C., 2015, ApJ, 798, L45
Venhola A. et al., 2018, A&A, 620, A165
Venhola A. et al., 2019, A&A, 625, A143
Villegas D. et al., 2010, ApJ, 717, 603
Voggel K., Hilker M., Richtler T., 2016, A&A, 586, A102
Weisz D. R. et al., 2011, ApJ, 743, 8
Young T., Jerjen H., López-Sánchez Á. R., Koribalski B. S., 2014, MNRAS, 444, 3052
Zanatta E. J. B., Sánchez-Janssen R., Chies-Santos A. L., de Souza R. S., Blakeslee J. P., 2021, preprint(arXiv:2103.02123)

SUPPORTING INFORMATION

Supplementary data are available at *MNRAS* online.

Table 1. Structural and photometric properties of the MATLAS dwarfs.
Table 4. Properties of the MATLAS nuclei.

Please note: Oxford University Press is not responsible for the content or functionality of any supporting materials supplied by the authors. Any queries (other than missing material) should be directed to the corresponding author for the article.

APPENDIX A: CONTAMINATION OF THE NUCLEI BY GLOBULAR CLUSTERS AND FOREGROUND STARS

A1 Globular clusters simulations

As mentioned in Section 5, we have estimated the probability for a globular cluster to be located at the centre of a dwarf and thus be visually confused with a compact central nucleus. For our calculation, we considered the sample of 425 nucleated dwarf galaxies with a diffuse part (masked nucleus) successfully modelled by a single Sérsic profile. Our estimation was done by running 1000 Monte

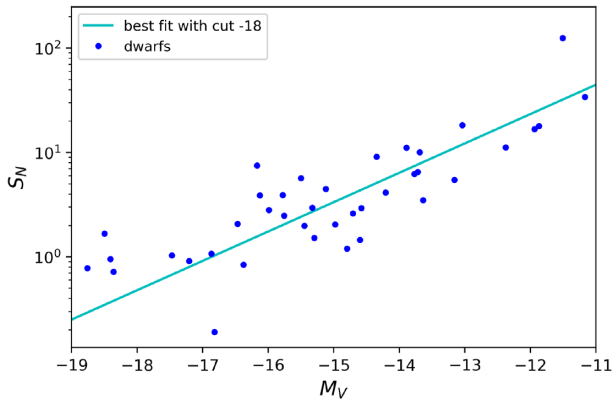

Figure A1. Relation between the specific frequency and the absolute magnitude in the V band for the sample of dwarfs from Georgiev et al. (2010). Blue dots represent the dwarfs. The formula for the best fit (cyan) is $\log(S_N) = 0.28M_V + 4.74$.

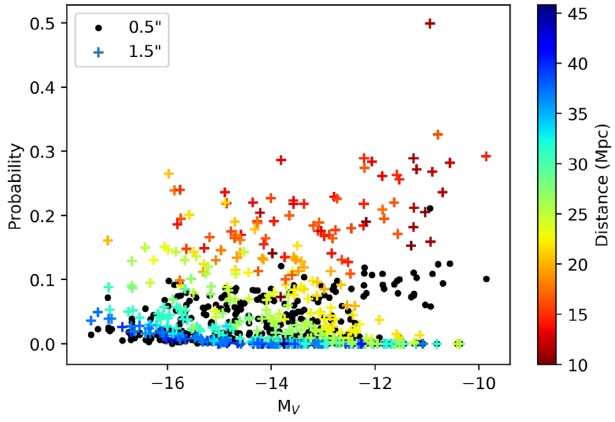

Figure A2. Probability to find a GC within a radius of 0.5 arcsec (black dots) and 1.5 arcsec (coloured crosses) as a function of the dwarf M_V. The colourbar shows the distance to the dwarf.

Carlo simulations for each of the dwarfs. The simulation randomly distributes GCs around dwarfs and look for the presence of at least one of them at the centre, within a defined radius, which in addition would be the brightest source at maximum distance of one effective radius.

As a first step, we need to estimate the specific frequency (S_N) and total number of GCs (N_{GC}) for each dwarf. We do not have a robust catalogue of GCs corrected from contamination for each dwarf, therefore we used the linear relation $\log(S_N)$ versus M_V found by Georgiev et al. (2010) for a sample of 73 dwarf galaxies (55 dIs, 5 dSphs, 3 dEs, and 5 Sm) in the field environment observed with the Advanced Camera for Surveys. In Fig. A1, we have plotted this relation and performed a linear regression on the data with a cut $M_V - 18$ to be consistent with the MATLAS dwarfs sample. We used the best fit, $\log(S_N) = 0.28M_V + 4.74$, to estimate the specific frequency of the MATLAS dwarfs coupled to the formula $S_N \equiv N_{GC}10^{0.4(M_V+15)}$ from Harris & van den Bergh (1981) to obtain the total number of GCs as a function of magnitude.

As a second step, now that we have an estimate of the total number of GCs for each dwarfs, given its absolute magnitude, we need to estimate the contamination by the GCs population from the host, i.e. the closest ETG. To do this, we have used catalogs of GCs for the MATLAS fields. These catalogues were available for the field of 86 per cent of the nucleated sample. We have computed the density of GCs in a ring area defined by two circles centered on the ETG with radii equal to the distance dwarf-ETG $\pm$ $3R_e$, i.e. the area of projection of the GCs on the dwarf. As a result, 7 per cent of the MATLAS nucleated dwarfs show a contamination by at least 1 GCs, with a maximum of 4 GCs. As the median contamination value is 0, we assume that the contamination is null for the dwarfs having no available catalogue.

The third step is to create the sample of GCs. To define the globular clusters luminosity function (GCLF), we assume a Gaussian distribution with $\mu = -7.4 + 0.04(M_V + 21.3)$ and $\sigma = 1.2 - 0.10(M_V + 21.3)$ (Jordán et al. 2006; Villegas et al. 2010; Harris, Harris & Alessi 2013). We pick randomly the GCs following the GCLF and remove the GCs with $m_g < 24.5$, the limit of detection of GCs in the MATLAS fields.

Our final step in this simulation is to project the GCs on the dwarf. We assume a spherical distribution and project the GCs within $3R_e$ around the dwarfs. We pick random spherical coordinates that we convert first to Cartesian 3D and then 2D coordinates. We consider a GC as a possible nucleus if it is situated at a certain distance (0.5 and 1.5 arcsec, see discussion below) to the photocentre of the galaxy and if it is the brightest source GC within one effective radius, to be consistent with our visual classification of our nucleated sample.

We present the results for the nucleated dwarfs considering separations of 0.5 and 1.5 arcsec in Fig. A2. In the case of a separation of 1.5 arcsec, we display the distance of the galaxy. The probability appears linked to the distance of the dwarf, with a higher probability for the closest dwarfs. This can be explained by the fact that the closer the dwarf, the larger the number of GCs visible. Thus, a robust sample of nucleated dwarfs with a probability of contamination $\lesssim$10 per cent can be defined by considering a maximum separation of 0.5 arcsec for the galaxies closer than 20 Mpc and a maximum separation of 1.5 arcsec for the more distant dwarfs.

A2 Galactic stars contamination

In our sample of nucleated dwarfs, the unresolved nuclei can easily be confused with Galactic stars. Therefore, we want to estimate the contamination of our nucleated sample by foreground (Galactic) stars. The *Gaia* mission of the European Space Agency (Gaia Collaboration 2016), with its observations of more than a billion stars located in and around the Milky Way, provide us with the data to estimate the level of contamination. We have cross-matched our sample of nucleated with the most recent catalogue, *Gaia* DR2 (Arenou et al. 2018; Gaia Collaboration 2018; Lindegren et al. 2018), with a maximum separation from the photocentre of 7 arcsec, the maximum separation observed for the MATLAS nuclei (Fig. 10). Of the 508 nucleated dwarfs, we obtained 58 matches (11 per cent). To ensure the stellar nature of the matched sources, we selected only the sources that have a proper motion value larger than the proper motion error. We find one object matching the position of a nucleus, allowing us to estimate a contamination of 0.2 per cent of our nucleated sample by foreground stars.

This paper has been typeset from a TEX/LATEX file prepared by the author.